

***In situ* oxygen-isotope, major-, and trace-element constraints on the metasomatic modification and crustal origin of a diamondiferous eclogite from Roberts Victor, Kaapvaal Craton**

Riches^{1*,†}, A. J. V., Ickert^{1,2}, R. B., Pearson¹, D. G., Stern¹, R. A., Jackson³, S. E., Ishikawa⁴, A., Kjarsgaard³, B. A., and Gurney⁵, J.J.

¹Department of Earth and Atmospheric Sciences, University of Alberta, Edmonton, AB, T6G 2E3, Canada.

²Scottish Universities Environmental Research Centre, Scottish Enterprise Technology Research Park, Rankine Avenue, East Kilbride, G75 0QF.

³Geological Survey of Canada, Ottawa, Canada

⁴Department of Earth Science and Astronomy, The University of Tokyo at Komaba, Tokyo, 153-8902, Japan.

⁵Department of Geological Sciences, University of Cape Town, Rondebosch, 7700, Republic of South Africa.

†Currently at: Department of Earth Sciences, University of Durham, Durham, DH1 3LE, United Kingdom.

*corresponding author: amy.j.riches@durham.ac.uk

phone: +44 191 33 42346

Accepted: *Geochimica et Cosmochimica Acta*

Draft: 16th November 2015

Keywords: Eclogite, Achaean Crust/Mantle, Subduction, Oxygen Isotopes, Diamond.

Word Count: 5,887 main text + 430 abstract

Figure Count: 8

Table Count: 0 (supplementary files)

Reference Total: 117

Appended Materials: Data table (Appendices A + B, excel), and supplementary text + figures (Appendix C)

1 Abstract (430 words)

2 A subducted oceanic crustal origin for most eclogite xenoliths in kimberlites has long been a
3 cornerstone of tectonic models for craton development. However, eclogite xenoliths often have
4 protracted and complex histories involving multiple metasomatic events that could overprint
5 some of the key geochemical indicators typically taken as evidence of a subducted origin (e.g,
6 garnet $\delta^{18}\text{O}$ -values and mineral $^{87}\text{Sr}/^{86}\text{Sr}$ compositions). To assess the potential for disturbance
7 of oxygen isotopic compositions in mantle eclogites via diamond-forming and other possible
8 metasomatic fluids, we have conducted a multi-technique *in situ* study of a diamondiferous
9 eclogite xenolith from the Roberts Victor kimberlite, S. Africa. Using SIMS we provide the first
10 texturally-controlled *in situ* measurements of $\delta^{18}\text{O}$ -values in eclogitic garnet in close proximity
11 to diamond.

12 Garnet and clinopyroxene modal proportions are heterogeneous in the xenolith and garnet
13 compositions vary from $\text{Mg}\# = 75.8\text{-}79.2$; grossular proportions = 8.05-10.14 mol. %, and
14 omphacitic pyroxene has Jd_{13-24} and $\text{Mg}\# = 86.6\text{-}90.0$. Rare earth element patterns of minerals
15 across the xenolith, including grains close to diamond, are typical LREE-depleted garnets and
16 markedly LREE-enriched pyroxenes. These silicate minerals also record detectable intra- and
17 inter-grain LREE abundance variations. Clinopyroxenes of the studied xenoliths show HFSE
18 and Sr abundance variations that are decoupled from LREE contents and major-element
19 variations.

20 Mineralogical constraints and bulk-rock reconstructions indicate that the studied sample
21 likely experienced selective incompatible element enrichment during small-volume ($\ll 0.03$ wt.
22 %) infiltration of metasomatic fluid(s) potentially linked to ancient diamond evolution. Intra-

23 grain major-element, LREE and HFSE variations in clinopyroxene resulted from late-stage
24 metasomatism. Oxygen isotope compositions in garnet are decoupled from all major- and trace-
25 element variations, with garnet $\delta^{18}\text{O}$ -values being uniform across the xenolith in a wide variety
26 of textural settings. Garnet $\delta^{18}\text{O}$ -values of $6.5 \pm 0.2 \text{ ‰}$ are higher than the mean ($5.19 \pm 0.26 \text{ ‰}$)
27 of the mantle garnet range (4.8-5.5 ‰).

28 Modelling of the buffering effect of mantle peridotite on CO_2 -rich and H_2O -rich
29 metasomatic fluids at temperatures within the diamond stability field indicates that the likelihood
30 of a metasomatic fluid with exotic oxygen isotopic composition arriving at a mantle eclogite
31 body with its isotopic composition unmodified, after percolative flow through dominantly
32 peridotitic mantle at great depth, is very low. As we find no evidence of metasomatically induced
33 garnet oxygen isotope variations in the studied diamondiferous eclogite xenolith we conclude
34 that the most likely origin for the elevated garnet $\delta^{18}\text{O}$ -values is via inheritance from a crustal
35 protolith altered at relatively low temperatures. These results have broader relevance and
36 support the hypothesis of a low-pressure protolith for mantle eclogite xenoliths, demonstrating
37 the robust nature of garnet oxygen isotope compositions – even in diamond-bearing eclogites.

38 **Keywords:** Eclogite, Achaean Crust/Mantle, Subduction, Oxygen Isotopes, Diamond.

39 **Main Text (5,727)**40 **1. Introduction**

41 The origins of kimberlite-borne eclogite xenoliths that are erupted through cratons have been
42 debated for the last 30 years or more (e.g., MacGregor and Manton, 1986; Hatton and Gurney,
43 1987; Jacob *et al.*, 1994; Beard *et al.*, 1996; Jacob and Foley, 1999; Schmidberger *et al.*, 2007;
44 Viljoen *et al.*, 2005; Aulbach *et al.*, 2007; Gurney *et al.*, 2010; Huang *et al.*, 2012; Shu *et al.*,
45 2014). Eclogites are volumetrically dominated by garnet and omphacitic pyroxene, and are
46 generally considered as meta-igneous rocks having broadly basaltic bulk-rock compositions.
47 Eclogites sampled as xenoliths preserve mineralogical and cryptic geochemical records of
48 complex and protracted lithospheric mantle histories (e.g., Heaman *et al.*, 2002, 2006). Broad
49 analogies have been drawn between mantle eclogite xenoliths sampled from depth and crustal
50 eclogites that generally occur in orogenic settings, but which have distinct metamorphic histories
51 (e.g., Coleman *et al.*, 1965; Nadaeu *et al.*, 1993; Baker *et al.*, 1997; Zack *et al.*, 2002; Zheng *et*
52 *al.*, 2003; Konrad-Schmolke *et al.*, 2008). Critically, the distribution of oxygen isotope
53 compositions of eclogite xenolith garnets, with $\delta^{18}\text{O}$ -values ranging significantly above and
54 below canonical mantle values, have drawn analogies with bulk-rock compositions reported for
55 shallow-level ophiolite and mid-ocean ridge basalt (MORB) sequences altered by fluids at
56 relatively low-temperatures. As such, these variations are often cited as evidence supporting a
57 recycled crustal origin (e.g., Jagoutz *et al.*, 1984; Neal and Taylor, 1990; Neal *et al.*, 1990;
58 Snyder *et al.*, 1995, 1997; Schulze *et al.*, 2000; Barth *et al.*, 2001; Jacob *et al.*, 2003; Spetsius *et*
59 *al.*, 2008; Riches *et al.*, 2010; Tappe *et al.*, 2011; Carmody *et al.*, 2013; Pernet-Fisher *et al.*,
60 2014). Prior studies of oxygen isotope compositions of eclogite garnets have, however, largely
61 employed multi-grain conventional-fluorination methods and laser-fluorination approaches on

62 mg-sized garnet fragments, which will result in compositional averages of larger garnet volumes.
63 In addition, garnet-clinopyroxene modal banding and wide-spread evidence for cryptic
64 metasomatism linked to the passage of incompatible-element-rich fluids \pm diamond occurrences
65 in eclogite xenoliths (e.g., Taylor *et al.*, 1996, 2000; Ishikawa *et al.*, 2008a-b; Spetsius and
66 Taylor, 2008; Liu *et al.*, 2009; Smart *et al.*, 2009) lead some scientists to question the primary
67 nature of garnet $\delta^{18}\text{O}$ -compositions (e.g., Huang *et al.*, 2014). The potential for eclogite garnet
68 oxygen isotope compositions being of metasomatic origin has profound implications for the
69 hypothesis of a subducted crustal origin for eclogite xenolith protoliths (e.g., Helmstaedt and
70 Doig; 1975; Jacob, 2004) and warrants further study.

71 To assess intra-sample garnet oxygen isotope homogeneity and thereby test the validity of
72 conclusions drawn from conventional- and laser-fluorination studies, which are considered
73 fundamental evidence supporting the subduction origin of mantle eclogites, we selected a
74 diamondiferous eclogite xenolith from the Roberts Victor kimberlite (**Fig. 1**) and utilised new
75 generation secondary-ion mass spectrometry (SIMS) to obtain highly precise *in situ* garnet
76 oxygen isotope data for texturally constrained grains at small spatial scales and low total
77 volumes (15 μm spot diameter of 1-2 μm depth; \ll 5 ng; e.g., Page *et al.*, 2010; Ickert and Stern,
78 2013). This sample exhibited significant variation in diamond content, silicate mineral texture
79 and mineral chemistry, enabling inter- and intra-grain garnet oxygen isotope variation to be
80 assessed in the context of macro- and grain-scale textural and mineral chemical variations.
81 Significantly, our study includes the first report of *in situ* $\delta^{18}\text{O}$ -compositions of garnet grains
82 adjacent to diamond in eclogite, allowing us to investigate the potential effects of diamond-
83 forming fluids on garnet oxygen isotope compositions. These data are supplemented by *in situ*

84 major- and trace-element abundance data of garnets and coexisting phases in garnet-rich and
85 clinopyroxene-rich portions of eclogite 09RV09 from the Roberts Victor kimberlite pipe.

86 **2. Analytical Methods**

87 **2.1 Sample preparation**

88 The studied eclogite xenolith, 09RV09 (total mass ~160 g), is from the Roberts Victor mine,
89 South Africa. The sample was selected on the basis of; 1) its relatively fresh appearance; 2) the
90 presence of diamonds, and; 3) heterogeneously distributed zones with varying modal proportions
91 of garnet and clinopyroxene. A 37 g slice derived from this diamondiferous-eclogite ([Fig. 2](#))
92 was used for our study. This carefully examined slice contains zones of varying
93 garnet:clinopyroxene modal proportion considered representative of bulk-rock modal variance.
94 To retain textural information during subsequent laser-ablation (LA)-ICP-MS and SIMS
95 analyses, garnets were extracted from a number of distinct zones in this xenolith slice using a 2.5
96 mm diamond-coated steel core drill prior to mounting in the central portion of a 25 mm epoxy
97 mount.

98 **2.2 *In situ* major- and trace-element characterisation**

99 All mineral major-, minor-, and trace-element abundances are reported in the
100 [supplementary materials](#) along with images of the studied sample regions. Mineral major-
101 element oxide abundances were determined by electron microprobe (EMP) analyses with a five
102 spectrometer Cameca SX-100 at the University of Alberta. All data were collected with a
103 focused (1 μm) 20 nA beam operating at 15 kV. Counting times for all elements were 20 to 30 s,
104 and standard PAP corrections were applied to all analyses using the software of [Armstrong](#)
105 ([1995](#)). Natural and synthetic standards were measured at intervals during each analytical

106 session to assess precision and accuracy. Element concentrations were always within 1 % of
107 accepted values. Detection limits (3σ above background) were typically ≤ 0.03 wt. % for Na_2O ,
108 MgO , CaO , NiO , and K_2O , ≤ 0.04 wt. % for Al_2O_3 , SiO_2 , TiO_2 , FeO , and V_2O_5 , and ≤ 0.05 wt. %
109 for MnO , P_2O_5 , and Cr_2O_3 . Additional information pertaining to the EMP methodology is
110 included in the [supplementary materials](#).

111 Garnet trace-element abundances were obtained at the Geological Survey of Canada,
112 Ottawa, using a Photon Machines Analyte 193 nm Ar-F excimer laser coupled to an Agilent
113 7700x quadrupole ICP-MS. Analyses were performed using a 10-16 Hz laser repetition rate at a
114 photon fluence of 4.4-7.0 Jcm^{-2} . Data were acquired with a 43 to 69 μm spot-size for garnets,
115 and a 52 μm spot for clinopyroxenes. Basaltic glass reference materials, USGS GSD-1G and
116 GSE-1G were utilized as primary standards, with a selection of in-house garnets as secondary
117 reference standards. Further analytical details are included in the [supplementary materials](#).

118 **2.3 Ion-probe oxygen isotope analyses**

119 All oxygen isotope compositions are reported relative to the Vienna Standard Mean Ocean
120 Water (VSMOW) standard. Where this can be described as:

$$121 \quad \delta^{18}\text{O}_{\text{VSMOW}} (\text{‰}) = \left[\left(\frac{^{18}\text{O}/^{16}\text{O}}{^{18}\text{O}/^{16}\text{O}} \right)_{\text{sample}} / \left(\frac{^{18}\text{O}/^{16}\text{O}}{^{18}\text{O}/^{16}\text{O}} \right)_{\text{VSMOW}} - 1 \right] * 1000.$$

122 For simplicity the VSMOW subscript is omitted and $\delta^{18}\text{O}$ notation is used in the text herein.

123 Oxygen isotope compositions of garnets were determined *in situ* with a Cameca IMS-1280
124 ion microprobe at the Canadian Centre for Isotopic Microanalyses (CCIM) at the University of
125 Alberta following procedures described by [Ickert and Stern \(2013\)](#). Calibration of the matrix
126 correction, as described by [Ickert and Stern \(2013; cf. Page et al., 2010\)](#), was conducted by

127 analysing a full suite of garnet working standards on a separate grain mount prior to analysing
128 the samples in this study. Seven 2.5 mm diameter cores of eclogite were mounted in a single 25
129 mm epoxy grain mount along with several chips of working standard UAG and secondary
130 standard S0088 (a Gore Mountain pyrope-almandine megacryst, and a Jeffrey Mine grossular,
131 respectively). All rock chips and garnets were within 0.5 cm of the centre of the grain mount.
132 Analyses were conducted in a single analytical session, using a 2.5-3.0 nA Cs primary beam with
133 a 15 μm spot diameter. Thirty analyses of UAG were interspersed at regular intervals among 94
134 sample points and seven analyses of S0088 (treated as an ‘unknown’) were collected during the
135 analytical session for quality assurance. This yielded an S0088 average $\delta^{18}\text{O}$ -value of $4.13 \pm$
136 0.09‰ (2σ), $n = 7$, which coincides with the mean reported in an independent study conducted
137 by [Ickert and Stern \(2013\)](#), indicating that the matrix correction is accurate. Total propagated
138 uncertainties (including calibration uncertainty) on each analytical point are $\pm 0.2\text{-}0.3 \text{‰}$ (2σ).
139 All data are reported in the [supplementary materials](#).

140 **3. Results**

141 **3.1 Petrographic characteristics**

142 In 09RV09, garnet-rich, and clinopyroxene-rich zones are unevenly distributed across the
143 $\sim 23 \text{ cm}^2$ surface area studied ([Fig. 2](#)). Larger (up to 5 mm in maximum dimension) garnet and
144 clinopyroxene crystals, with well-developed lamellar pyroxene, and garnet exsolution,
145 respectively, account for $\sim 5\text{-}10 \%$ of the studied eclogite surface. These large clinopyroxene
146 crystals are turbid in appearance and generally exhibit narrow ($< 750 \mu\text{m}$) sponge-textured rims
147 texturally analogous to those reported for some Bellsbank eclogites (e.g., [Taylor and Neal,](#)
148 [1989](#)). The remaining surface area is dominated by rounded interlocking grains (generally 2-3

149 mm in maximum dimension) of garnet and clinopyroxene. Minor interstitial phases include
150 phlogopite (up to 1 mm in maximum dimension), sulphide (generally < 500 μm maximum
151 dimension), graphite (<650 μm), diamond (up to 800 μm in the studied portions of 09RV09), and
152 anhedral clinopyroxene (generally <700 μm). Narrow veins (<150 μm) and cracks (<10 μm) on
153 grain boundaries and penetrating larger crystals contain trapped melt (~60-80 vol. %) with lesser
154 amounts of K-rich phlogopite (≤ 50 μm), clinopyroxene (≤ 20 μm), and small needles of Ti-oxide
155 and sulphide (<1 μm wide, up to 8 μm in length). Utilising the textural classification of
156 [MacGregor and Carter \(1970\)](#), the sample is a Group I eclogite. Notably, other accessory
157 mineral phases, for example apatite \pm magnesite \pm monazite \pm kyanite \pm coesite \pm dolomite,
158 which have been observed in other eclogite xenoliths ([Sobolev et al., 1994](#); [Snyder et al., 1998](#))
159 and carbonated high-pressure experimental assemblages ([Knoche et al., 1999](#); [Dasgupta et al.,](#)
160 [2004](#)) are absent from the studied sample.

161 Zones rich in garnet have garnet-clinopyroxene ratios of ~90:10 to ~70:30, whereas
162 clinopyroxene-rich zones have garnet-clinopyroxene ratios of ~10:90 to ~30:70. Petrographic
163 study and X-ray tomography ([supplementary materials](#)) show that abundances and spatial
164 distributions of accessory phlogopite, sulphide, and diamond are not directly correlated with one
165 another, and these do not vary in a systematic manner with garnet and clinopyroxene modal
166 abundances.

167 **3.2 Mineral major- and trace-element abundances**

168 *In situ* mineral major- and trace-element abundances of 09RV09 are reported in the
169 [supplementary materials](#) where reasoning for the use of the geometric form of trace-element
170 anomalies throughout this text is discussed. Clinopyroxenes are characterised by Mg# values of

171 86.6-90.0 (where $Mg\# = 100Mg/[Mg+Fe^{total}]$) and jadeite contents that generally range from 13-
172 24 mol. %. Clinopyroxene TiO_2 abundances range from 0.16-0.29 wt. %, Cr_2O_3 contents vary
173 from <0.05-0.21 wt. %, and K_2O concentrations are generally 0.18-0.29 wt. %, with only two
174 data points at sponge-textured clinopyroxene rims recording <0.04 wt. % K_2O . These
175 clinopyroxene compositions are broadly similar to those reported for other diamondiferous and
176 textural Group I eclogites (e.g., [Jacob, 2004](#); [Smart et al., 2009](#)).

177 Garnet compositions show small to moderate intra- and inter-grain major-element variation
178 with $Mg\#$ of 75.8 to 79.2 and $Ca\#$ of 8.2 to 10.4 (where $Ca\# = 100Ca/[Ca+Mg+Fe^{total}]$), with no
179 consistent trend observed in core to rim traverses. These garnets have low Cr_2O_3 contents (≤ 0.25
180 wt. %), low $Cr\#$ values (< 0.70 , where $Cr\# = 100Cr/[Cr+Al]$), combined $FeO^{total} + CaO$ contents
181 of 13.0-16.6 wt. %, and Na_2O contents ≤ 0.10 wt. %. This range of garnet major-element
182 compositions ([Fig. 3a-b](#)) overlaps that reported for textural Group I and Group II eclogites (\pm
183 diamond; [McCandless and Gurney, 1989](#)). Garnet compositions of 09RV09 are broadly
184 consistent with the Group-A garnet major-element classification of [Taylor and Neal \(1989\)](#).

185 Despite significant modal mineral variation, the silicate major-element characteristics of
186 09RV09 do not record the type of systematic mineral compositional variations found to
187 accompany variations in garnet-clinopyroxene proportions in some other modally variable
188 Roberts Victor eclogites. For instance, a diamondiferous eclogite xenolith containing exsolved
189 spinel ($< 200 \mu m$; RVSA-71, [Ishikawa et al., 2008a-b](#)) and a diamondiferous spinel-free eclogite
190 (HRV-247; [Hatton, 1978](#); [O'Reilly and Griffin, 1995](#); [Ishikawa et al. 2008a](#)) showed variations
191 in clinopyroxene jadeite contents, and grossular proportions in garnet that were lower in
192 clinopyroxene-rich zones while the $Mg\#$ of both of these phases was lower in garnet-rich zones.

193 Chondrite normalised rare-earth-element (REE) abundances of 09RV09 garnets are LREE-
194 depleted relative to HREE ($[La/Yb]_N = 0.001-0.019$, where N denotes normalisation to CI-
195 chondrite; **Fig. 4a**). Primitive mantle normalised trace-element abundance patterns (**Fig. 4b**)
196 display negative Sr- and Ti-anomalies (generally 0.10-0.40 and 0.27-0.47, respectively). In
197 detail, 09RV09 garnets show moderate variations in LREE abundances (e.g., La = 6-70 ppb), Ti,
198 and Hf (88-1386 ppm, and 70-900 ppb, respectively), but little to no variation beyond analytical
199 uncertainties in HREE, Y, Sc, V, and Zr contents (**supplementary materials**). Abundances of
200 Ti and Hf do not co-vary with La, and La abundances in excess of 20 ppb are restricted to three
201 data points for a single grain distal from zones with the most extreme garnet:clinopyroxene
202 values. The time-resolved ablation signals for these data points do not show resolvable inclusion
203 signals and these La contents are, therefore, considered to represent either a combination of
204 volumetrically minor, finely-disseminated, and evenly distributed LREE-enriched inclusions in
205 the sampled volume, or higher LREE abundances truly intrinsic to this grain. Notably, all
206 09RV09 garnet data points are characterised by little to no Eu-anomaly beyond analytical
207 uncertainties ($[Eu/Eu^*]_N = 1.0-1.4$ and relative errors of 9-21 %, 2σ).

208 In contrast to garnet, all 09RV09 clinopyroxene analyses are LREE-enriched ($[La/Yb]_N =$
209 $8.52-29.2$). These clinopyroxenes lack detectable Eu-anomalies, have positive Sr-anomalies
210 (2.4-4.7), negative Ti-anomalies (0.24-0.42; **Fig. 4b**), and are generally characterised by positive
211 $[Zr/Hf]_{PM}$ values (0.50-0.70) and Ti, V and Sc abundances show little or no variation beyond
212 analytical uncertainties. Detectable variations are present in clinopyroxene LREE, MREE
213 HREE, Y, Sr, Zr, Hf, Nb, and Ta abundances; of these the LREE strongly correlate with one
214 another and HFSE are strongly or very strongly correlated (e.g., **supplementary materials**).
215 However, comparison of clinopyroxene LREE, Sr, and HFSE abundances shows that these

216 element groups, and Sr, do not co-vary as high degrees of scatter are evident ($R^2 \leq 0.3$).
217 Correlations of LREE with MREE, Y, and HREE are moderate to weak, and uncertainties on
218 MREE, HREE, and Y abundances limit confident interpretations of these relationships.
219 Significantly, no strong correlations are evident when abundances of LREE, Sr, Zr, Hf, Nb, and
220 Ta in clinopyroxene are compared with La contents of texturally associated garnet (not plotted
221 here).

222 The range of garnet and clinopyroxene trace-element abundances and inter-element
223 fractionations determined for 09RV09 are broadly analogous to those reported for other Mg-rich
224 eclogites (e.g., [Barth et al., 2002](#); [Smart et al., 2009](#)). [Gréau et al. \(2011\)](#) suggested that
225 clinopyroxene trace-element criteria differ between textural Group I and Group II eclogites
226 thereby extending the earlier classification scheme of [McCandless and Gurney \(1989\)](#);
227 comparison with recently recommended discrimination criteria shows that 09RV09
228 clinopyroxene Zr abundances are consistent with the Group I classification of [Gréau et al \(2011\)](#).
229 On the other hand, Sr and Nd contents of 09RV09 clinopyroxene (472-835 ppm, 7.2-14 ppm,
230 respectively) are higher than other Group I eclogites, and corresponding Ti and Zr abundances
231 vary over a range (with associated uncertainties) that overlaps both Group I and Group II
232 characteristics of [Gréau et al., \(2011\)](#). This chemical variability undermines a simple
233 classification scheme based on trace-elements but also emphasises the suitability of sample
234 09RV09 for studying the effects of metasomatic processes on oxygen isotope compositions.
235 Critically, garnets and clinopyroxenes of 09RV09 do not exhibit systematic variations in the
236 trace-element abundances determined for regions with differing garnet:clinopyroxene modal
237 proportions, and abundances and inter-element ratios of trace-elements, which cover a wide-

238 range of geochemical properties, do not correlate systematically with major-element
239 concentrations, Mg#, and/or garnet grossular contents (e.g., [Fig. 5a](#)).

240 **3.3 Garnet oxygen-isotope compositions**

241 *In situ* oxygen isotope compositions of 94 analytical points in 7 garnets derived from
242 texturally distinct locations in 09RV09 yield $\delta^{18}\text{O}$ -values of +6.2-6.8 ‰ with no detectable
243 variation outside total analytical uncertainties. The mean, mode, and median of these garnet
244 oxygen isotope compositions are coincident at +6.5 ‰ ([Fig. 6a](#)). The garnet $\delta^{18}\text{O}$ -values show
245 negligible variations, while some major- and trace-element contents vary moderately. However,
246 there is no systematic correlation between garnet oxygen isotope compositions and major-, and
247 trace-element characteristics of 09RV09 garnets and clinopyroxenes at scales ranging from 10's
248 μm to many cm ([supplementary materials](#)).

249 The probability of the mean garnet $\delta^{18}\text{O}$ -value of 09RV09 being equal to that of the mean of
250 the mantle garnet $\delta^{18}\text{O}$ -distribution is low. Results of t-tests to compare 09RV09 garnet $\delta^{18}\text{O}$ -
251 data with that of [Mattey et al., \(1994\)](#) assuming garnet fractionation factors of <0.5 ‰ for
252 olivine, orthopyroxene, and clinopyroxene, yield a very low probability ($p < 0.001$) of coincident
253 means in all cases (where t-tests include; 1) the Shapiro-Wilk approach that assumes both
254 datasets are derived from normally distributed populations; and, 2) non-parametric Kolmogorov-
255 Smirnov tests, including the Lilliefors correction, with assumptions of both equal and unequal
256 variances applied during each t-test). In addition, Mann-Whitney Rank sum tests of these data
257 also show that the mean of our garnet $\delta^{18}\text{O}$ -data is significantly different from garnet-equilibrium
258 values calculated for mantle mineral laser-fluorination data reported by [Mattey et al. 1994](#) (p
259 <0.001).

260 4. Discussion

261 Constraining the origin of mantle eclogite xenoliths is of fundamental importance to studies
262 of craton origin and evolution. Isotopic compositions (O, Mg, Pb-Pb, Sm-Nd, Lu-Hf, and Re-
263 Os) reported for a number of diamondiferous and non-diamondiferous eclogite xenoliths of the
264 Roberts Victor kimberlite suggest that these materials are derived from Archean subducted crust
265 (e.g., [Kramers, 1979](#); [McGregor and Manton, 1986](#); [Pearson *et al.*, 1995](#); [Shirey *et al.*, 2001](#);
266 [Jacob *et al.*, 2005](#); [Wang *et al.*, 2012](#)). A recent study of mineral major- and trace-element
267 characteristics and garnet $\delta^{18}\text{O}$ -compositions of 33 eclogite xenoliths from the Roberts Victor
268 Mine ([Gréau *et al.*, 2011](#)), and an investigation of a single texturally complex eclogite (RV07-17;
269 [Huang *et al.*, 2014](#)), have questioned the robust nature of garnet $\delta^{18}\text{O}$ -values as tracers of a
270 crustal precursor for eclogites; these authors suggested that oxygen isotopes are markedly
271 fractionated by mantle metasomatic processes. In particular, [Gréau *et al.* \(2011\)](#) suggested that
272 garnet $\delta^{18}\text{O}$ -values are correlated with clinopyroxene incompatible element abundances, arguing
273 that garnet oxygen isotope compositions reflect carbonatite metasomatism. Our detailed
274 investigation of 09RV09 provides an important data-set to evaluate the robustness of garnet
275 oxygen isotope compositions to metasomatic processes.

276 4.1 Metasomatic modification of 09RV09

277 Metasomatic modification of 09RV09 is evident in the form of late-stage infiltration along
278 garnet and clinopyroxene grain boundaries (generally <150 μm wide) and narrow cracks (<10
279 μm) penetrating coarse-sized (2-3mm) garnets and clinopyroxenes. These narrow features
280 contain trapped melt (~60-80 vol. % of the infiltration zones) with lesser amounts of K-rich
281 phlogopite ($\leq 50 \mu\text{m}$), clinopyroxene ($\leq 20 \mu\text{m}$), and small needles of Ti-oxide and sulphide (<1

282 μm wide, up to $8 \mu\text{m}$ in length) and are interpreted as metasomatic in origin. In some cases,
283 needle-like phases ($<5\mu\text{m}$ in length) have nucleated at the grain boundaries of large, pre-existing,
284 garnet and clinopyroxene and have grown outwards into narrow infiltration zones (**Fig. 7a**).

285 Larger phlogopite grains (up to $500 \mu\text{m}$) in 09RV09 generally occur at the point where several
286 narrow ($<1 \text{ mm}$ wide) infiltration zones connect to one another. Though textural observations
287 alone make it difficult to fully assess the genetic origin of these phases, we consider large
288 phlogopites as crystals formed during metasomatic infiltration experienced by 09RV09; this
289 interpretation is consistent with previous suggestions of a metasomatic origin for phlogopites of
290 other Roberts Victor eclogite xenoliths (e.g., [Ongley et al., 1987](#)). The relatively high K_2O
291 contents (generally $>0.20 \text{ wt. } \%$) of 09RV09 clinopyroxenes are within the range reported for
292 other textural Group I diamondiferous eclogite xenoliths (e.g., [McCandless and Gurney, 1989](#))
293 and eclogitic clinopyroxene inclusions in diamond (e.g., [Taylor et al., 1998, 2000](#); [Stachel and](#)
294 [Harris, 2008](#) and references therein). Previous studies (e.g., [Hatton, 1978](#); [Gréau et al., 2011](#))
295 have suggested that clinopyroxene K_2O contents above $0.07 \text{ wt. } \%$ are indicative of metasomatic
296 modification associated with diamond formation in mantle environments, and these studies
297 generally show elevated Na_2O contents ($>0.09 \text{ wt. } \%$) in garnet accompanying the high K
298 concentrations in clinopyroxene (e.g., [Hatton, 1978](#)). Further, 09RV09 clinopyroxenes preserve
299 notable inter- and intra-grain heterogeneity in the form of LREE, MREE, Sr, Ti and Nb
300 abundances. In contrast, 09RV09 garnets are generally characterised by intra-grain major- and
301 trace-element homogeneity and generally have Na_2O contents $<0.09 \text{ wt. } \%$. These garnets have
302 higher Ti abundances compared with some - not all - textural Group II eclogites (**supplementary**
303 **materials**), but lower Ti contents than mean and median values of eclogitic garnet diamond
304 inclusions (e.g., [Stachel and Harris, 2008](#)).

305 The number of diamonds ($>100\ \mu\text{m}$) observed *in situ* is small ($n = 7$), but those identified
306 occur in regions of intersecting infiltration zones (\pm adjacent phlogopite). The uneven
307 distribution of 09RV09 diamonds, and their occurrence in interstitial regions, is consistent with
308 observations reported for other diamondiferous eclogite xenoliths (e.g., [Anand et al., 2004](#);
309 [Spetsius and Taylor, 2008](#)). However, the clear evidence for metasomatic modification of
310 09RV09 makes it imperative that potential evidence of the protolith is treated cautiously.

311 **4.1.1 Element exchange processes at the grain-scale**

312 The disparate degree of equilibration exhibited by 09RV09 clinopyroxenes and garnets
313 testifies to differing element exchange behaviours in these phases (cf., [Burton et al., 1995](#);
314 [Taylor et al., 1996](#)) with respect to the metasomatic history of this sample. An end-member
315 model developed here specifically for 09RV09 references theories of diamond formation and
316 takes account of regional tectonomagmatic events likely to have affected materials in proximity
317 to the Colesburg Lineament, and sampled by the Cretaceous Roberts Victor kimberlite proximal
318 to that major intra-cratonic terrane boundary ([Fig. 1](#)). Our model involves two metasomatic
319 events influencing a garnet-clinopyroxene protolith after incorporation into the lithospheric
320 mantle; the first being ancient and involving metasomatism at great depth by carbon-bearing
321 fluids facilitating diamond formation broadly synchronous with stabilisation of the Kaapvaal
322 Craton >2.5 Ga (see [Pearson and Wittig, 2008](#); [Helmstaedt et al., 2010](#); [Shu and Brey, 2015](#)) and
323 potentially concurrent with suturing along the Colesburg Lineament at ~ 2.9 Ga ([Schmitz et al.,](#)
324 [2004](#); [Shu et al., 2013](#)). This ancient metasomatism is followed by elemental and isotopic
325 equilibration of silicate phases during protracted high-pressure, high-temperature residence in
326 lithospheric mantle. Magnesium may be introduced during ancient metasomatism, and/or a
327 small degree of melt removal may be facilitated by fluid introduction (where melt removal is

328 anticipated to cause only a small shift to lower $\delta^{18}\text{O}$ -values; [Williams et al., 2009](#)). Thus, the
329 relatively magnesian nature of this sample and the homogenous but higher Mg# of garnet in
330 close proximity to diamond ([Fig. 3b](#)) may be, at least in part, related to an ancient metasomatic
331 event. The second modification event in our model scenario involves a late-stage metasomatic
332 interaction linked to kimberlite arrival and xenolith entrainment at ~ 124 Ma ([Smith et al., 1985](#))
333 contributing to frozen records of inter- and intra-grain heterogeneity in 09RV09 clinopyroxenes.
334 Assessing the validity of this model requires consideration of the nature of element exchange in
335 eclogitic garnets and omphacitic pyroxenes ([supplementary materials](#)). For example, the intra-
336 grain homogeneity displayed by 09RV09 garnets may reflect relatively fast element exchange
337 and equilibration of major- and trace-element abundances in garnet during a single metasomatic
338 event when compared with co-existing clinopyroxene. Alternatively, element exchange
339 processes in garnet may be orders of magnitude slower than those operating in clinopyroxene
340 leading to the conclusion that the garnets retain robust records of their mantle protolith that are
341 resistant to late-stage small-volume metasomatic modification.

342 Equilibration temperatures calculated for clinopyroxene cores and coexisting garnets in
343 09RV09 are within the range anticipated for cratonic lithospheric mantle materials resident at
344 depths in which diamond is stable. Given this observation, we reason that 09RV09 garnet
345 compositions reflect equilibrated mantle compositions minimally disturbed by late-stage small-
346 volume metasomatism. In contrast, trivalent LREE-MREE, tetravalent HFSE, and divalent
347 cations of small ionic radius (e.g., Fe, Mg, Mn) may have diffused relatively rapidly in the outer
348 portions of 09RV09 clinopyroxenes as a result of recent metasomatic disturbance. The observed
349 decoupling between REE and HFSE in 09RV09 clinopyroxenes likely relate to differences in the
350 rate or nature of REE and HFSE element exchange in clinopyroxene, potentially high HFSE

351 blocking temperatures, and/or sequestering of HFSE by volumetrically minor rutile needles
352 crystallised in corresponding metasomatic infiltration zones. It is likely that all of these factors
353 contributed during metasomatic modification of 09RV09 clinopyroxenes.

354 **4.1.2 Bulk-rock reconstruction and its constraints on 09RV09 metasomatism**

355 The precise nature of fluids that infiltrated 09RV09, related to diamond formation, and
356 kimberlite entrainment, is not well constrained at this time (e.g., speciation, fO_2 , isotopic
357 characteristics). Given the similarities between 09RV09 silicate trace-element characteristics
358 and those of silicate diamond inclusion data (e.g., Ireland *et al.*, 1994; Taylor *et al.*, 1996, 2000;
359 Sobolev *et al.*, 1998; Stachel *et al.*, 2004), metasomatic agents that have influenced 09RV09
360 likely resemble the spectrum of compositions reported for diamond fluid inclusions. For these
361 reasons, we model the trace-element composition resulting from mixing between possible
362 protolith compositions and anticipated metasomatic fluids. Modification by kimberlite
363 (generally considered to be CO₂-rich and LREE-enriched; e.g., Becker and Le Roux, 2006;
364 Kjarsgaard *et al.*, 2009) and/or potential LREE-enriched fluids derived from the host kimberlite
365 is possible, but is considered to be volumetrically minor.

366 Bulk-rock reconstructions utilise representative garnet and clinopyroxene trace-element core
367 compositions, trace-element characteristics of altered gabbro (e.g., Hart *et al.*, 1999; Bach *et al.*,
368 2001) previously considered by others as a possible eclogite protolith (e.g., Green and
369 Ringwood, 1967), and trace-element compositions reported for gem-quality diamond (McNeill *et*
370 *al.*, 2009) and fluid inclusions of fibrous diamonds (Klein-BenDavid *et al.*, 2010). Results of
371 these calculations indicate that the addition of <<0.03 wt. % of a diamond-forming incompatible-
372 element-rich fluid to an oceanic crustal protolith can account for the LREE-enrichment

373 calculated for the reconstructed bulk-rock compositions of 09RV09 (**Fig. 7b** and **supplementary**
374 **materials**). The addition of similarly low metasomatic fluid proportions ($\ll 0.05$ wt. %) is
375 required if the potential crustal protolith is considered to be derived from a more magnesian
376 (relative to typical gabbro) sheeted dyke complex lacking Eu-anomalies (not shown) and/or an
377 altered basalt of broadly picritic/komatiitic composition (cf., [Shirey et al., 2001](#)). Given this
378 evidence for metasomatic modification of 09RV09, we appraise the consequences for our
379 interpretation of the homogeneous garnet $\delta^{18}\text{O}$ -compositions in this xenolith.

380 **4.2 Oxygen-isotope signatures: metasomatism versus precursor inheritance**

381 In contrast to the prevailing paradigm, it has been suggested that eclogite garnet oxygen
382 isotope compositions in excess of the typical garnet mantle range may reflect secondary
383 overprinting by the passage of carbonatitic melt (e.g., [Gréau et al., 2011](#)), and/or could reflect
384 interaction with CO-, OH, and/or CO₂-bearing fluids (e.g., [Deines et al., 1991](#)) similar to those
385 reported for diamond inclusions (e.g., [Navon et al., 1988](#); [Turner et al., 1990](#); [Izraeli et al., 2001](#);
386 [Klein-BenDavid, 2004, 2007](#); [Tomlinson et al., 2006](#)) and observed in some mantle xenoliths
387 transported by alkali basalts (e.g., [Bergman and Dubessy, 1984](#); [Andersen and Neumann, 2001](#)).
388 There are no oxygen isotopic determinations on primary carbonatites erupted in an un-modified
389 state from the mantle with which to test this conjecture. Current experimental, empirical, and
390 theoretical partition coefficients combined with fractionation factors reported for basaltic liquids
391 and associated phases at temperatures of ~ 1000 - 1300°C (cf., [Eiler, 2001](#) and [Chacko et al., 2001](#))
392 indicate that silicate $\delta^{18}\text{O}$ -values vary by <0.5 ‰ during the generation and fractional
393 crystallisation of basaltic melts at high-temperatures (1000 - 1300°C). In addition, pressure effects
394 on isotopic exchange at crustal and upper-mantle conditions are thought to be small due to
395 limited volume changes (<0.005 ‰ for pressure differences of 20-30 kbar; e.g., [Clayton et al.,](#)

396 1975; Polyakov and Kharlashina, 1994). Glass, CO, OH, and CO₂ species may fractionate δ¹⁸O-
397 compositions by detectable amounts (>>0.5 ‰; Deines *et al.*, 1991), but the effect of possible
398 solutes, and their potential speciation variations, on oxygen isotope fractionation in mantle fluids
399 carrying gaseous molecules is not well constrained at conditions appropriate for mantle
400 environments (e.g., O'Neil, 1986; Bindeman, 2008 and references therein). Zheng (1993)
401 suggested that, under certain circumstances, partial substitution of [OH]₄⁻⁴ for [SiO₄]⁻⁴ in
402 grossular molecules could potentially lead to ¹⁸O-enrichment, and Kohn and Valley (1998)
403 proposed that octahedral cation substitutions may also influence garnet δ¹⁸O-values. Oxygen
404 diffuses slowly in garnet even under hydrous conditions (e.g., Lichtenstein and Hoernes, 1992;
405 Cole and Chakraborty, 2001). For these reasons, and considering mass-balance requirements,
406 kinetic processes such as diffusion, and/or solution-precipitation, associated with metasomatic
407 exchange in mantle environments will potentially lead to disequilibrium characteristics in the
408 form of garnet compositional zoning developed during complex multi-stage histories (e.g.,
409 Zhang *et al.*, 2000) anticipated for SCLM residence times up to Gyrs.

410 Given the complex metasomatic history of sample 09RV09 we might expect to see some
411 measureable small-scale variations in oxygen isotope compositions that, for instance, relate to
412 elemental or textural variation. No variation in garnet δ¹⁸O-values exists. The data are within
413 measurement uncertainty both within garnet grains and in garnets across the entire xenolith.
414 Similarly, garnets in a coesite-rutile-bearing eclogite from Roberts Victor with abundant veinlets
415 (sample 13-64-136), also lack inter- and intra-grain variation in garnet δ¹⁸O-compositions
416 (Russell *et al.*, 2013). These observations contrast to inter-sample garnet δ¹⁸O variance reported
417 for a texturally complex eclogite (RV07-17; Huang *et al.*, 2014). Moreover, there is no
418 correlation at all between clinopyroxene incompatible element abundances such as La and garnet

419 $\delta^{18}\text{O}$ -values for 09RV09 (**Fig. 5b**), indicating that incompatible-element enrichment due to
420 metasomatism is unlikely to be the primary control on the oxygen isotopic composition of this
421 eclogite. This result means that a metasomatic origin of the statistically non-robust correlation
422 between La and $\delta^{18}\text{O}$ -values presented by Gréau *et al.* (2010; **Fig. 5b**) is unlikely ($p < 0.001$). No
423 valid mixing curve is evident in the combined data set, especially considering that the Group II
424 eclogites included in the Gréau *et al.* (2010) are part of a separate group of eclogites from
425 Roberts Victor whose $\delta^{18}\text{O}$ -values range to above +6 ‰; e.g., Ongley *et al.*, 1987). This
426 consideration weakens the argument for metasomatic overprinting of garnet $\delta^{18}\text{O}$ -compositions
427 and hence the existing and new eclogite data plotted on this co-variation diagram, therefore, is
428 not able to provide a unique solution to account for eclogitic garnet $\delta^{18}\text{O}$ -compositions.

429 Mass balance considerations with respect to garnet oxygen isotope compositions (where
430 oxygen is a major-element) offer a more powerful argument in that to significantly modify the
431 oxygen isotopic composition over 1 ‰ away from the canonical mantle value requires
432 equilibration with substantially larger relative volumes of fluid (or unrealistic $\delta^{18}\text{O}$ -
433 compositions) than can be accounted for by the degree of trace-element modification in 09RV09.
434 A metasomatic model postulated to drive volumetrically significant ^{18}O enrichments (or
435 depletions) in eclogite garnet $\delta^{18}\text{O}$ -compositions requires that a highly reactive, volatile-rich
436 agent traverse substantial quantities of mantle without equilibrating with the ambient material.
437 Mass balance (“closed system”) and Rayleigh (“open system”) models (e.g., **Fig. 8**; Taylor,
438 1977; Criss and Taylor, 1986) place constraints on the degree of fluid-rock interaction required
439 to buffer a fluid with an initial $\delta^{18}\text{O}$ -value of +7.5 ‰. In these models, we utilised forsterite-
440 calcite and calcite- CO_2 oxygen isotope fractionation factors (yielding $\Delta\text{CO}_2\text{-forsterite} = +4.1$ ‰;
441 Chiba *et al.*, 1989; Chacko *et al.*, 1991) and a calcite- H_2O fractionation factor (giving $\Delta\text{H}_2\text{O}$ -

442 forsterite = +0.3 ‰; O'Neil et al., 1969; Friedman and O'Neil, 1977). At an assumed
443 temperature of 1100 °C, a closed-system model predicts that 1 g of a fluid, rich in H₂O or CO₂,
444 requires 15-20 grams of peridotite (approximated by forsterite = +5.0 ‰) to become buffered to
445 a composition within ±0.5 ‰ of the median peridotitic mantle value. Under open-system
446 conditions, which may provide a more realistic analogue for mantle metasomatism, fluid
447 interaction with substantially less peridotite for a given fluid volume (<1:5 fluid-rock ratio) is
448 required to buffer the fluid δ¹⁸O-value to the composition of silicate mantle with which it is
449 interacting. These models show that only minor fluid-rock interaction is required to buffer the
450 oxygen isotope composition of a mantle metasomatic fluid. To generate the 09RV09 garnet
451 δ¹⁸O-value of +1 ‰ above the mantle value, and up to +3.5 ‰ observed in other eclogites,
452 mantle pyroxenites and diamond inclusions (MacGregor and Manton, 1986; Pearson et al., 1991;
453 Jacob et al., 2003; Ickert et al., 2015) requires not only that very high fluid-rock ratios (≥2:5;
454 Fig. 8) are maintained for a compositionally extreme fluid at the local “sample scale” but that
455 these extreme δ¹⁸O-compositions are continuously maintained from the fluid source, throughout
456 its flow at great depth (asthenospheric and/or lithospheric mantle), where the fluid flow regime is
457 likely percolative. Therefore, the probability of a metasomatic fluid with an extreme oxygen
458 isotope composition surviving unmodified during transport through the mantle, itself dominantly
459 peridotitic, and imposing this signature on an eclogite body within the peridotite is very low
460 indeed. This clearly favours the interpretation of 09RV09 garnet δ¹⁸O-values as representing a
461 robust tracer of the protolith lithology rather than the product of mantle metasomatism.

462 Evaluating the suggestion that diamond-forming fluids in general may be responsible for
463 generating exotic mantle oxygen isotopic compositions (Gréau et al. 2011) we note that 6
464 peridotite suite garnets included in diamonds analysed by Matthey et al. (1994) have a mean δ¹⁸O-

465 value of +5.3 ‰, identical to typical mantle peridotite. Hence, there is no solid evidence for
466 appreciable oxygen isotope modification in garnet-bearing mantle materials during
467 metasomatism by small-volume incompatible-element enriched fluids. Indeed, it is more likely
468 that $\delta^{18}\text{O}$ -compositions of small-degree metasomatic fluids equilibrate with the host rock and,
469 thus, we reason that mantle eclogites and peridotites impart their oxygen isotope signature on
470 volumetrically minor and transient fluids during metasomatism and diamond evolution.

471 **4.3 Summary and implications**

472 To critically appraise the nature of potential metasomatic signatures in mantle eclogite
473 xenoliths, we conducted a multi-technique *in situ* study of a diamondiferous eclogite xenolith
474 with varying garnet:clinopyroxene proportions (09RV09) from the Roberts Victor kimberlite, S.
475 Africa. We provided the first *in situ* measurements of $\delta^{18}\text{O}$ -values in eclogitic garnet in close
476 proximity to diamond, and retaining textural control, to test theories concerned with metasomatic
477 modification of eclogites during diamond formation, particularly garnet oxygen isotope
478 compositions.

479 Intra-grain variations in clinopyroxene major-element, LREE-MREE and HFSE contents
480 appear to have resulted from later metasomatism related to kimberlite arrival and xenolith
481 entrainment, yet oxygen isotope compositions in garnet are uniform, within tight analytical
482 uncertainties, across the xenolith in a wide variety of textural settings. SIMS garnet $\delta^{18}\text{O}$ -values
483 of 6.5 ± 0.2 ‰ are higher than the mean mantle garnet range (4.8-5.5 ‰). There is no co-
484 variation of oxygen isotope composition with incompatible element based indicators of
485 metasomatism.

486 The lack of detectable inter- and intra-grain oxygen isotope variation in 09RV09 garnet,
487 including garnet in close proximity to diamond, indicates that garnet $\delta^{18}\text{O}$ -compositions are
488 ancient and likely not affected by infiltration of diamond-forming fluids. The intra-sample garnet
489 oxygen isotope homogeneity of 09RV09 is of particular interest as available data suggest that
490 intra-sample garnet oxygen isotope homogeneity is likely representative of mantle eclogites in
491 general. Prior laser-fluorination (LF) studies of garnet separates have generally shown highly
492 reproducible eclogite garnet $\delta^{18}\text{O}$ -compositions within a given sample both at individual
493 laboratories and in inter-laboratory comparison studies (e.g., [Rumble et al., 2007](#)). Furthermore,
494 results of other recent *in situ* studies of garnet $\delta^{18}\text{O}$ -compositions of 52 other eclogite xenoliths
495 have demonstrated intra-sample homogeneity ([Russell et al., 2013](#); [Smit et al., 2014](#); [Dongre et al., 2015](#))
496 with only one known exception; RV07-17 ([Huang et al., 2014](#)). Our data, combined
497 with the slow time-scales of oxygen isotopic diffusion in the mantle (cf., [Russell et al., 2013](#)) and
498 the difficulties in moving metasomatic fluids with exotic oxygen isotopic compositions through
499 the Earth's mantle without buffering their compositions to the mantle $\delta^{18}\text{O}$ -value support the
500 concept that eclogite oxygen isotope compositions largely reflect their crustal precursors.

501 The oxygen isotope composition of garnets in 09RV09 is significantly different from typical
502 mantle values supporting a crustal origin for its precursor and in line with many other studies of
503 Roberts Victor eclogite xenoliths and eclogitic diamond inclusions (e.g., [MacGregor and
504 Manton, 1986](#); [Jacob et al., 2005](#); [Tappert et al., 2005](#); [Schulze et al., 2013](#); [Ickert et al., 2013](#),
505 [2015](#)), irrespective of their textural groupings.

506 **5. Acknowledgements**

507 Funding to DGP supported this research and was provided by the CERC programme. Sergei
508 Matveev is thanked for his assistance during electron microprobe analyses. Three anonymous
509 reviewers and the Associate Editor, Dmitri A. Ionov, are thanked for constructive suggestions
510 that have helped to improve this manuscript.

511 7. References

- 512 Anand M., Taylor L. A., Misra K. C., Carlson W. D., and Sobolev N. V. (2004). Nature of diamonds in
513 Yakutian eclogites: views from eclogite tomography and mineral inclusions in diamonds. *Lithos*,
514 77(1), 333-348.
- 515 Andersen T., and Neumann E.R., 2001. Fluid inclusions in mantle xenoliths. *Lithos*, 55(1), 301-320.
- 516 Armstrong, J.T., (1995). A package of correction programs for the quantitative electron microbeam X-ray
517 analysis of thick polished materials, thin films, and particles. *Microbeam Anal.*, 4, 177-200.
- 518 Aulbach S., Pearson N.J., O'Reilly S.Y., and Doyle B.J., 2007. Origins of xenolithic eclogites and
519 pyroxenites from the Central Slave Craton, Canada. *J. Petrol.* 48, 1843–1873.
- 520 Bach W., Alt J.C., Niu Y., Humphris S.E., Erzinger J., and Dick H.J.B., 2001. The geochemical
521 consequences of late-stage low-grade alteration of lower ocean crust at the SW Indian Ridge: results
522 from ODP Hole 735B (Leg 176). *Geochim. Cosmochim. Acta.*, 65, 3267–3287.
- 523 Baker J., Matthews A., Matthey D., Rowley D., and Xue F., 1997. Fluid-rock interactions during ultra-high
524 pressure metamorphism, Dabie Shan, China. *Geochim. Cosmochim. Acta*, 61(8), 1685-1696.
- 525 Barth M.G., Rudnick R.L., Horn I., McDonough W.F., Spicuzza M.J., Valley J.W., and Haggerty S.E.,
526 2001. Geochemistry of xenolithic eclogites from West Africa, part I: a link between low MgO
527 eclogites and Archean crust formation. *Geochim. Cosmochim. Acta*, 65 (9), 1499–1527.
- 528 Barth M.G., Rudnick R.L., Horn I., McDonough W.F., Spicuzza M.J., Valley J.W., and Haggerty S.E.,
529 2002. Geochemistry of xenolithic eclogites from West Africa, part 2; Origins of the high MgO
530 eclogites. *Geochim. et Cosmochim. Acta*, 66(24), 4325-4345.
- 531 Beard B.L., Fraccini K.N., Taylor L.A., Snyder G.A., Clayton R.A., Mayeda T.K., and Sobolev N.V.,
532 1996. Petrography and geochemistry of eclogites from the Mir kimberlite, Yakutia, Russia. *Contrib.*
533 *Mineral. Petrol.*, 125, 293-310.
- 534 Becker M., and Le Roex A. P., 2006. Geochemistry of South African on- and off-craton, Group I and
535 Group II kimberlites: petrogenesis and source region evolution. *J. Petrol.*, 47(4), 673-703.
- 536 Bergman S.C., and Dubessy J., 1984. CO₂-CO fluid inclusions in a composite peridotite xenolith:
537 implications for upper mantle oxygen fugacity. *Contrib. Mineral. Petrol.*, 85(1), 1-13.
- 538 Bindeman I., 2008. Oxygen isotopes in mantle and crustal magmas as revealed by single crystal analysis.
539 *Rev. Mineral. Geochem.*, 69(1), 445-478.
- 540 Burton, K. W., Kohn, M. J., Cohen, A. S., and O'Nions, R. K., 1995. The relative diffusion of Pb, Nd, Sr
541 and O in garnet. *Earth Planet. Sci. Lett.*, 133(1), 199-211.

- 542 Caporuscio F.A., 1990. Oxygen isotope systematics of eclogite mineral phases from South Africa. *Lithos*,
543 25, 203-210.
- 544 Carmody L., Barry P.H., Shervais J.W., Kluesner J.W., and Taylor L.A., 2013. Oxygen isotopes in
545 subducted oceanic crust: A new perspective from Siberian diamondiferous eclogites. *Geochem.*
546 *Geophys. Geosyst.*, 14(9), doi: 10.1002/ggge.20220.
- 547 Chacko T., Cole D.R., and Horita J., 2001. Equilibrium oxygen, hydrogen and carbon isotope
548 fractionation factors applicable to geologic systems. *Rev. Mineral. Geochem.*, 43(1), 1-81.
- 549 Chacko T., Mayeda T. K., Clayton R. N., and Goldsmith J. R., 1991, Oxygen and carbon isotope
550 fractionations between CO₂ and calcite. *Geochim. Cosmochim. Acta*, 55(10), 2867-2882.
- 551 Chiba H., Chacko T., Clayton R. N., and Goldsmith J. R., 1989, Oxygen isotope fractionations involving
552 diopside, forsterite, magnetite, and calcite: Application to geothermometry. *Geochim. Cosmochim.*
553 *Acta*, 53(11), 2985-2995.
- 554 Clayton R.N., Goldsmith J.R., Karel K.J., Mayeda T K., and Robert C.N., 1975. Limits on the effect of
555 pressure on isotopic fractionation. *Geochim. Cosmochim. Acta*, 39(8), 1197-1201.
- 556 Cole D.R., and Chakraborty S., 2001. Rates and mechanisms of isotopic exchange. *Rev. Mineral.*
557 *Geochem.*, 43(1), 83-223.
- 558 Coleman R. G., Lee D. E., Beatty L. B., and Brannock W. W., 1965. Eclogites and eclogites: their
559 differences and similarities. *Geol. Soc. Am. Bullet.*, 76(5), 483-508.
- 560 Criss R. E., and Taylor Jr. H. P., 1986, Meteoric-hydrothermal systems. *Rev. Mineral.*, 16, 373-424.
- 561 Dasgupta R., Hirschmann M. M., and Withers A. C., 2004. Deep global cycling of carbon constrained by
562 the solidus of anhydrous, carbonated eclogite under upper mantle conditions. *Earth Planet. Sci. Lett.*,
563 227(1), 73-85.
- 564 Deines P., Harris J.W., Robinson, D.N., Gurney, J.J., and Shee, S.R., 1991. Carbon and oxygen isotope
565 variations in diamond and graphite eclogites from Orapa, Botswana, and the nitrogen content of their
566 diamonds. *Geochim. et Cosmochim. Acta*, 55(2), 515-524.
- 567 Dongre A. N., Jacob D. E., and Stern R. A., 2015. Subduction-related origin of eclogite xenoliths from
568 the Wajrakarur kimberlite field, Eastern Dharwar craton, Southern India: Constraints from petrology
569 and geochemistry. *Geochim. Cosmochim. Acta*, 166, 165-188.
- 570 Eiler J.M., 2001. Oxygen isotope variations of basaltic lavas and upper mantle rocks. *Rev. Mineral.*
571 *Geochem.*, 43(1), 319-364.
- 572 Friedman I., and O'Neil, J. R., 1977, Compilation of stable isotope fractionation factors of geochemical
573 interest. In *Data of Geochemistry 6th Ed.*, (Vol. 440). US Govt., Washington, USA.
- 574 Garlick G.D., MacGregor I.D., and Vogel D.E., 1971. Oxygen isotope ratios in eclogites from
575 kimberlites. *Science*, 172, 1025-1027.
- 576 Gréau Y., Huang J.-X., Griffin W.L., Renac C., Alard O., and O'Reilly S.Y., 2011. Type I eclogites from
577 Roberts Victor kimberlites: Products of extensive mantle metasomatism. *Geochim. Cosmochim. Acta*,
578 75, 6927-6954.
- 579 Green D. H., and Ringwood A. E., 1967. An experimental investigation of the gabbro to eclogite
580 transformation and its petrological applications. *Geochimica et Cosmochimica Acta*, 31(5), 767-833.

- 581 Gregory R.T., and Taylor Jr. H.P., 1981. An oxygen isotope profile in a section of Cretaceous oceanic
582 crust, Samail ophiolite, Oman: Evidence for $\delta^{18}\text{O}$ buffering of the oceans by deep (>5 km) seawater-
583 hydrothermal circulation at mid-ocean ridges. *J. Geophys Res*, 86(B4), 2737-2755.
- 584 Gurney, J. J., Helmstaedt, H. H., Richardson, S. H., and Shirey, S. B., 2010. Diamonds through time.
585 *Econ. Geol.*, 105(3), 689-712.
- 586 Hart S.R., Blusztain J., Dick H.J.B., Meyer P.S., and Muehlenbachs K., 1999. The fingerprint of seawater
587 circulation in a 500-meter section of ocean crust gabbros. *Geochim. Cosmochim. Acta.*, 63, 4059-
588 4080.
- 589 Hatton C.J., 1978. The geochemistry and origin of xenoliths from the Roberts Victor Mine. *PhD thesis*,
590 *Univ. Cape Town, Cape Town, South Africa*.
- 591 Hatton C.J., and Gurney J.J., 1987. Roberts Victor eclogites and their relation to the mantle. In: Nixon
592 P.H. (Ed.), *Mantle Xenoliths*, Wiley, Chichester, pp. 453-463
- 593 Heaman L.M., Creaser R.A., and Cookenboo H.O., 2002. Extreme enrichment of high field strength
594 elements in Jericho eclogite xenoliths: A cryptic record of Paleoproterozoic subduction, partial
595 melting, and metasomatism beneath the Slave craton, Canada. *Geology*, 30(6), 507-510.
- 596 Heaman L.M., Creaser R.A., Cookenboo H.O., and Chacko T., 2006. Multi-stage modification of the
597 Northern Slave mantle lithosphere: evidence from zircon-and diamond-bearing eclogite xenoliths
598 entrained in Jericho kimberlite, Canada. *J. Petrol.*, 47(4), 821-858.
- 599 Helmstaedt H., and Doig, R., 1975. Eclogite nodules from kimberlite pipes of the Colorado Plateau –
600 samples of subducted Franciscan-type oceanic lithosphere. *Phys. Chem. Earth*, 9, 95-111.
- 601 Helmstaedt, H. H., Gurney, J. J., and Richardson, S. H., 2010. Ages of cratonic diamond and lithosphere
602 evolution: constraints on Precambrian tectonics and diamond exploration. *Can. Min.*, 48(6), 1385-
603 1408.
- 604 Huang J.-X., Gréau Y., Griffin W.L., O'Reilly S.Y, and Pearson N.J., 2012. Multi-stage origin of Roberts
605 Victor eclogites: Progressive metasomatism and its isotopic effects. *Lithos*, 142-143, 161-181.
- 606 Huang J.-X., Griffin W.L., Gréau Y., Pearson N.J., O'Reilly S.Y., Cliff J., and Martin L., 2014.
607 Unmasking xenolithic eclogites: Progressive metasomatism of a key Roberts Victor sample. *Chem.*
608 *Geol.*, 364, 56-65.
- 609 Ickert R.B., and Stern R.A., 2013. Matrix corrections and error analysis in high-precision SIMS $^{18}\text{O}/^{16}\text{O}$
610 measurements of Ca-Mg-Fe garnet. *Geostand. Geoanal. Res.*, 37(4), 429-448.
- 611 Ickert R.B., Stachel T., Stern R. A., and Harris, J. W., 2013. Diamond from recycled crustal carbon
612 documented by coupled $\delta^{18}\text{O}$ - $\delta^{13}\text{C}$ measurements of diamonds and their inclusions. *Earth Planet. Sci.*
613 *Lett.*, 364, 85-97.
- 614 Ireland T.R., Rudnick R.L., and Spetsius Z., 1994. Trace elements in diamond inclusions from eclogites
615 reveal link to Archean granites. *Earth Planet. Sci. Lett.*, 128(3), 199-213.
- 616 Ishikawa A., Pearson D.G., Maruyama S., Cartigny P., Ketchum R.A., and Gurney J.J., 2008a.
617 Compositional layering in a highly diamondiferous eclogite xenolith from the Roberts Victor
618 kimberlite, South Africa and its implications for diamond genesis. *IX International Kimberlite Conf.*,
619 Abst. No. 9IKC-A-00078.

- 620 Ishikawa A., Pearson D.G., Maruyama S., de Bruin D., and Gurney J.J., 2008b. Compositional variability
621 of the Roberts Victor eclogites: evidence for mantle metasomatism involving diamond dissolution. *IX*
622 *International Kimberlite Conf.*, Abst. No. 9IKC-A-00079.
- 623 Izraeli E.S., Harris J.W., and Navon O., 2001. Brine inclusions in diamonds: a new upper mantle fluid.
624 *Earth Planet. Sci. Lett.*, 187(3), 323-332.
- 625 Jacob D., 2004. Nature and origin of eclogite xenoliths in kimberlites. *Lithos*, 77, 295–316.
- 626 Jacob D., and Jagoutz E., 1994. A diamond-graphite bearing eclogitic xenolith from Roberts Victor
627 (South Africa): Indications for petrogenesis from Pb-, Nd-, and Sr-isotopes. *In: Meyer H.O.A.,*
628 *Leonardos O.H. (Eds), Kimberlites, Related Rocks, and Mantle Xenoliths. Companhia de Pesquisa de*
629 *Recursos Minerais, Spec. Pub. vol. 1/A, pp. 304-317.*
- 630 Jacob D., and Foley S.F., 1999. Evidence for Archean ocean crust with low high field strength element
631 signature from diamondiferous eclogite xenoliths. *Lithos*, 48, 317-336.
- 632 Jacob D., Jagoutz E., Lowry D., Matthey D., and Kudrjajtseva G., 1994. Diamondiferous eclogites from
633 Siberia: remnants of Archean oceanic crust. *Geochim. Cosmochim. Acta*, 58(23), 5191-5207.
- 634 Jacob D.E., Schmickler B., and Schulze D.J., 2003. Trace element geochemistry of coesite-bearing
635 eclogites from the Roberts Victor Kimberlite. *Lithos*, 71, 337-351.
- 636 Jacob D., Bizimis M., and Salters V.J.M., 2005. Lu-Hf and geochemical systematics of recycled ancient
637 oceanic crust: evidence from Roberts Victor eclogites. *Contrib. Mineral. Petrol.*, 148(6), 707-720.
- 638 Jagoutz E., Dawson J.B., Hoernes S., Spettel B., and Wanke H., 1984. Anorthositic oceanic crust in the
639 Archean Earth. *XV Lunar Planet. Sci. Conf.*, pp. 395-396.
- 640 Kjarsgaard B. A., Pearson D. G., Tappe S., Nowell G. M., and Dowall D. P., 2009. Geochemistry of
641 hypabyssal kimberlites from Lac de Gras, Canada: comparisons to a global database and applications
642 to the parent magma problem. *Lithos*, 112, 236-248.
- 643 Klein-BenDavid O., Izraeli E.S., Hauri E., and Navon O., 2004. Mantle fluid evolution—a tale of one
644 diamond. *Lithos*, 77(1), 243-253.
- 645 Klein-BenDavid O., Izraeli E.S., Hauri E., and Navon O., 2007. Fluid inclusions in diamonds from the
646 Diavik mine, Canada and the evolution of diamond-forming fluids. *Geochim. et Cosmochim. Acta*,
647 71(3), 723-744.
- 648 Klein-BenDavid O., Pearson D.G., Nowell G.M., Ottley C., McNeill J.C., and Cartigny P., 2010. Mixed
649 fluid sources involved in diamond growth constrained by Sr–Nd–Pb–C–N isotopes and trace elements.
650 *Earth Planet. Sci. Lett.*, 289(1), 123-133.
- 651 Knoche R., Sweeney R. J., and Luth R. W. (1999). Carbonation and decarbonation of eclogites: the role
652 of garnet. *Contrib. Mineral. Petrol.*, 135(4), 332-339.
- 653 Kohn M.J., and Valley J.W., 1998. Effects of cation substitutions in garnet and pyroxene on equilibrium
654 oxygen isotope fractionations. *J. Meta. Geol.*, 16(5), 625-639.
- 655 Konrad-Schmolke M., Zack T., O'Brien P.J., and Jacob D.E., 2008. Combined thermodynamic and rare
656 earth element modelling of garnet growth during subduction: Examples from ultrahigh-pressure
657 eclogite of the Western Gneiss Region, Norway. *Earth Planet. Sci. Lett.*, 272(1), 488-498.
- 658 Kramers J.D., 1979. Lead, uranium, strontium, potassium and rubidium in inclusion-bearing diamonds
659 and mantle-derived xenoliths from southern Africa, *Earth Planet. Sci. Lett.*, 42, 58-70.

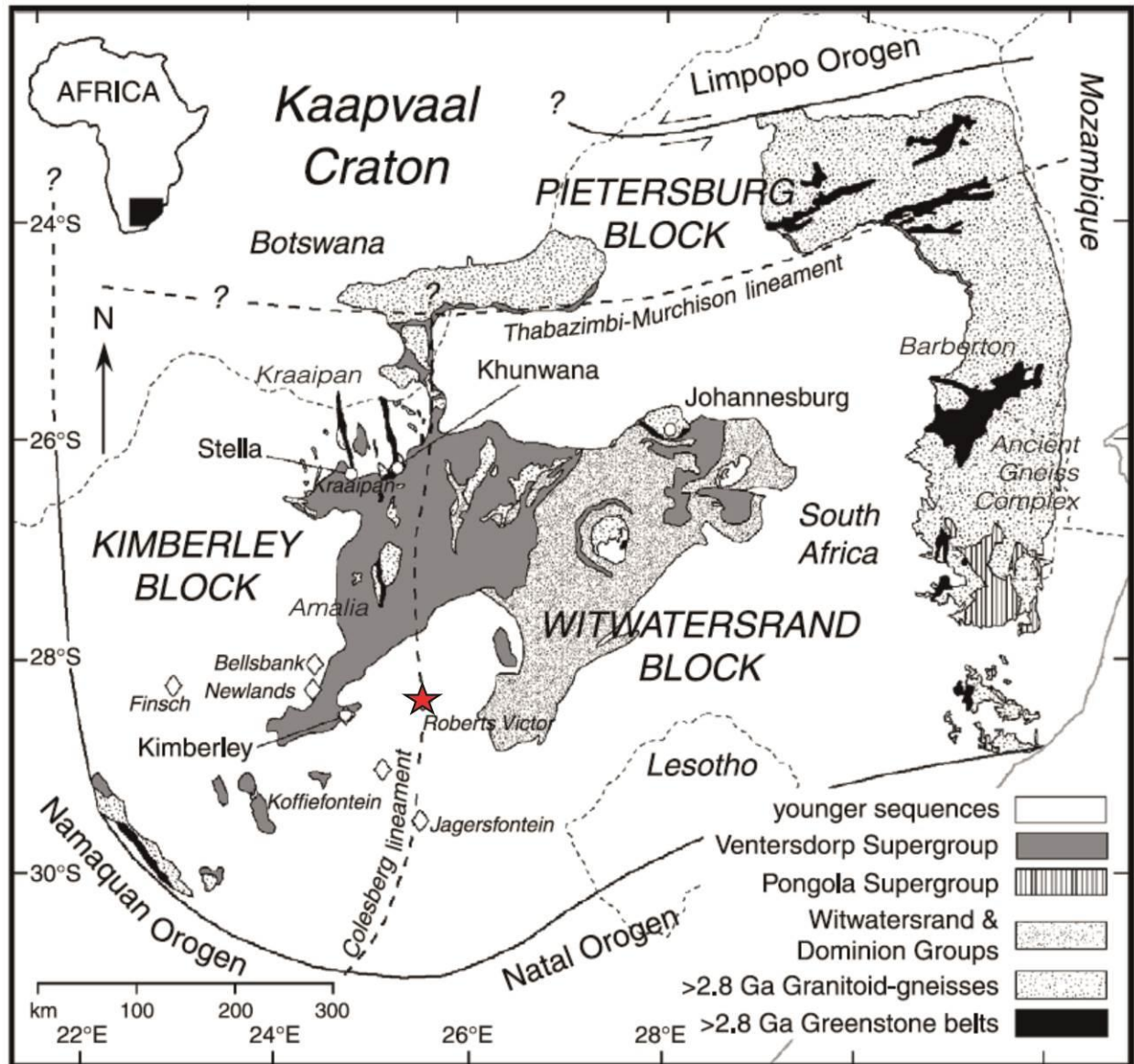
- 660 MacGregor I.D., and Carter J.L., 1970. The chemistry of clinopyroxenes and garnets of eclogite and
661 peridotite xenoliths from the Roberts Victor Mine, South Africa. *Phys. Earth Planet. Interiors*, 3, 391-
662 397.
- 663 MacGregor I.D., and Manton W.I., 1986. Roberts Victor Eclogites: Ancient Oceanic Crust. *J. Geophys.*
664 *Res.*, 91(B14), 14,063-14,079.
- 665 Matthey D., Lowry D., and Macpherson C. (1994). Oxygen isotope composition of mantle peridotite.
666 *Earth Planet. Sci. Lett.*, 128(3), 231-241.
- 667 McCandless T.E., and Gurney J.J., 1989. Sodium in garnet and potassium in clinopyroxene; criteria for
668 classifying mantle eclogites. In: Ross J, (Ed) *Kimberlites and related rocks. Their mantle/crustal*
669 *setting, diamonds and diamond exploration*, vol. 2, Blackwell, Carlton, Australia, pp. 827-832.
- 670 McNeill J., Pearson D.G., Klein-BenDavid O., Nowell G.M., Ottley C.J., and Chinn I., 2009. Quantitative
671 analysis of trace element concentrations in some gem-quality diamonds. *J. Phys. Cond. Matt.*, 21(36),
672 364207.
- 673 Navon O., Hutcheon I.D., Rossman G.R., and Wasserburg G.J., 1988. Mantle-derived fluids in diamond
674 micro-inclusions. *Nature*, 355, 784-789.
- 675 Neal C.R., and Taylor L.A., 1990. Comment on "Mantle eclogites: evidence of igneous fractionation in
676 the mantle" by J.R Smyth, F.A. Caporuscio, and T.C. McCormick. *Earth Planet. Sci. Lett.*, 101, 112-
677 119.
- 678 Neal C.R., Taylor L.A., Davidson J.P., Holden P., Halliday A.N., Nixon P.H., Paces J.B., Clayton R.N.,
679 and Mayeda T.K., 1990. Eclogites with oceanic crustal and mantle signatures from the Bellsbank
680 kimberlite, South Africa, part 2: Sr, Nd, and O isotope geochemistry. *Earth Planet. Sci. Lett.*, 99, 362-
681 379.
- 682 O'Neil J. R., 1986. Theoretical and experimental aspects of isotopic fractionation. *Rev. Mineral.*
683 *Geochem.*, 16(1), 1-40.
- 684 O'Neil J. R., Clayton R. N., and Mayeda T. K., 1969. Oxygen isotope fractionation in divalent metal
685 carbonates. *J. Chem. Phys.*, 51, 5547-5558.
- 686 O'Reilly S.Y., and Griffin W.F., 1995. Trace-element partitioning between garnet and clinopyroxene in
687 mantle-derived pyroxenites and eclogites: P-T-X controls. *Chem. Geol.*, 121(1-4), 105-130.
- 688 Ongley J.S., Basu A.R., and Kyser T.K., 1987. Oxygen isotopes in coexisting garnets, clinopyroxenes and
689 phlogopites of Roberts Victor eclogites: implications for petrogenesis and mantle metasomatism.
690 *Earth Planet. Sci. Lett.*, 83, 80-84.
- 691 Page F.S., Kita N. T., and Valley J.W., 2010. Ion microprobe analyses of oxygen isotopes in garnets of
692 complex chemistry. *Chem. Geol.*, 270, 9-19.
- 693 Pearson D. G., and Wittig N., 2008. Formation of Archaean continental lithosphere and its diamonds: the
694 root of the problem. *J. Geol. Soc.*, 165(5), 895-914.
- 695 Pearson D. G., Davies G. R., Nixon P. H., Greenwood P. B., and Matthey D. P. 1991, Oxygen isotope
696 evidence for the origin of pyroxenites in the Beni Bousera peridotite massif, North Morocco:
697 derivation from subducted oceanic lithosphere. *Earth Planet. Sci. Lett.*, 102(3), 289-301.
- 698 Pearson D. G., Snyder G. A., Shirey S. B., Taylor L. A., Carlson R. W., and Sobolev N. V., 1995.
699 Archaean Re-Os age for Siberian eclogites and constraints on Archaean tectonics. *Nature*, 374(6524),
700 711-713.

- 701 Pernet-Fisher J.F., Howarth G.H., Liu Y., Barry P.H., Carmody L., Valley J.W., Bodnar R.J., Spetsius
702 Z.V., and Taylor L. A., 2014. Komsomolskaya diamondiferous eclogites: evidence for oceanic crustal
703 protoliths. *Contrib. Min. Petro.*, 167(3), 1-17.
- 704 Polyakov V.B., and Kharlashina N.N., 1995. The use of heat capacity data to calculate carbon isotope
705 fractionation between graphite, diamond, and carbon dioxide: a new approach. *Geochim. Cosmochim.*
706 *Acta*, 59(12), 2561-2572.
- 707 Riches A.J.V., Liu Y., Day J.M.D., Spetsius Z.V., and Taylor L.A., 2010, Subducted Oceanic Crust As
708 Diamond Hosts Revealed By Garnets Of Mantle Xenoliths From Nyurbinskaya, Siberia, *Lithos*,
709 120(3-4), 368-378.
- 710 Rumble D., Miller M. F., Franchi I. A., and Greenwood R. C., 2007. Oxygen three-isotope fractionation
711 lines in terrestrial silicate minerals: An inter-laboratory comparison of hydrothermal quartz and
712 eclogitic garnet. *Geochim. Cosmochim. Acta*, 71(14), 3592-3600.
- 713 Russell A.K., Kitajima K., Strickland A., Medaris Jr. L.G., Schulze D.J., and Valley J.W., 2013. Eclogite-
714 facies fluid infiltration: constraints from $\delta^{18}\text{O}$ zoning in garnet. *Contrib. Mineral. Petrol.*, 165, 103-
715 116.
- 716 Schmidberger S. S., Simonetti A., Heaman L. M., Creaser R. A., and Whiteford S., 2007. Lu–Hf, *in situ*
717 Sr and Pb isotope and trace element systematics for mantle eclogites from the Diavik diamond mine:
718 Evidence for Paleoproterozoic subduction beneath the Slave craton, Canada. *Earth Planet. Sci. Lett.*,
719 254(1), 55-68.
- 720 Schmitz M. D., Bowring S. A., de Wit M. J., and Gartz V., 2004. Subduction and terrane collision
721 stabilize the western Kaapvaal craton tectosphere 2.9 billion years ago. *Earth Planet. Sci Lett.*, 222(2),
722 363-376.
- 723 Schulze D.J., Valley J.W., and Spicuzza M.J., 2000. Coesite eclogites from the Roberts Victor kimberlite,
724 South Africa. *Lithos*, 54, 23-32.
- 725 Schulze, D. J., Harte, B., Page, F. Z., Valley, J. W., Channer, D. M. D., and Jaques, A. L., 2013.
726 Anticorrelation between low $\delta^{13}\text{C}$ of eclogitic diamonds and high $\delta^{18}\text{O}$ of their coesite and garnet
727 inclusions requires a subduction origin. *Geology*, 41(4), 455-458.
- 728 Smart K.A., Heaman L.M., Chacko T., Simonetti A., Kopylova M., Mah D., and Daniels D., 2009. The
729 origin of high-MgO diamond eclogites from the Jericho Kimberlite, Canada. *Earth Planet. Sci. Lett.*,
730 284, 527-537.
- 731 Smit K. V., Stachel T., Creaser R. A., Ickert R. B., DuFrane S. A., Stern R. A., and Seller M., 2014.
732 Origin of eclogite and pyroxenite xenoliths from the Victor kimberlite, Canada, and implications for
733 Superior craton formation. *Geochim. Cosmochim. Acta*, 125, 308-337.
- 734 Snyder G.A., Taylor L.A., Jerde E.A., Clayton R.N., Mayeda T.K., Deines P., Rossmann G.R., and
735 Sobolev N.V., 1995. Archean mantle heterogeneity and the origin of diamondiferous eclogites,
736 Siberia: Evidence from stable isotopes and hydroxyl in garnet. *Amer. Min.*, 80, 799-809.
- 737 Snyder G.A., Taylor L.A., Crozaz G., Halliday A.N., Beard B.L., Sobolev V.N., and Sobolev N.V., 1997.
738 The origins of Yakutian eclogite xenoliths. *J. Petrol.*, 38 (1), 85–113.
- 739 Snyder G. A., Taylor L. A., Beard B. L., Crozaz G., Halliday A. N., Sobolev V. N., and Sobolev N. V.,
740 1998. Reply to a comment by D. Jacob et al. on ‘The Origins of Yakutian Eclogite Xenoliths’. *J.*
741 *Petrol.*, 39(8), 1535-1543.

- 742 Shirey S.B., Carlson R.W., Richardson S.H., Menzies A., Gurney J.J., Pearson D.G., Harris J.W., and
743 Wiechert U., 2001. Archean emplacement of eclogitic components into lithospheric mantle during
744 formation of the Kaapvaal Craton. *Geophys. Res. Lett.*, 28(13), 2509-2512.
- 745 Shu Q., and Brey G. P., 2015. Ancient mantle metasomatism recorded in subcalcic garnet xenocrysts:
746 Temporal links between mantle metasomatism, diamond growth and crustal tectonomagmatism. *Earth
747 Planet. Sci. Lett.*, 418, 27-39.
- 748 Shu Q., Brey G. P., Gerdes A., and Hofer H. E., 2014. Mantle eclogites and garnet pyroxenites—the
749 meaning of two-point isochrons, Sm–Nd and Lu–Hf closure temperatures and the cooling of the
750 subcratonic mantle. *Earth Planet. Sci. Lett.*, 389, 143-154.
- 751 Shu Q., Brey G. P., Gerdes A., and Hofer H. E., 2013. Geochronological and geochemical constraints on
752 the formation and evolution of the mantle underneath the Kaapvaal craton: Lu–Hf and Sm–Nd
753 systematics of subcalcic garnets from highly depleted peridotites. *Geochim Cosmochim Acta*, 113, 1-
754 20.
- 755 Sobolev V. N., Taylor L. A., Snyder G. A. and Sobolev N. V., 1994. International Geological Congress,
756 Beijing: University of Beijing, Diamondiferous eclogites from the Udachnaya kimberlite pipe, p. 359.
757 Yakutia. *Int. Geol. Rev.*, 36, 42–64
- 758 Sobolev N.V., Snyder G.A., Taylor L.A., Keller R.A., Yefimova E.S., Sobolev V.N., and Shimizu N.,
759 1998. Extreme chemical diversity in the mantle during eclogitic diamond formation: evidence from 35
760 garnet and 5 pyroxene inclusions in a single diamond. *Int. Geol. Rev.*, 40(7), 567-578.
- 761 Spetsius Z.V., and Taylor L.A., 2008. Diamonds of Siberia: photographic evidence for their origin.
762 Knoxville, TN: Tranquility Base Press, pp 278.
- 763 Spetsius Z.V., Taylor L.A., Valley J.W., Deangelis M.T., Spicuzza M., Ivanov A.D., and Banzerak V.I.,
764 2008. Diamondiferous xenoliths from crustal subduction: garnet oxygen isotopes from the
765 Nyurbinskaya pipe, Yakutia. *Euro. J. Mineral.*, 20, 375–385.
- 766 Stachel T., and Harris J.W., 2008. The origin of cratonic diamonds—constraints from mineral inclusions.
767 *Ore Geol. Rev.*, 34(1), 5-32.
- 768 Stachel T., Aulbach S., Brey G.P., Harris J.W., Leost I., Tappert R., and Viljoen K.S. 2004. The trace
769 element composition of silicate inclusions in diamonds: a review. *Lithos*, 77(1), 1-19.
- 770 Tappe S., Smart K. A., Pearson D. G., Steenfelt A., and Simonetti A., 2011. Craton formation in Late
771 Archean subduction zones revealed by first Greenland eclogites. *Geology*, 39(12), 1103-1106.
- 772 Tappert R., Stachel T., Harris J. W., Muehlenbachs K., Ludwig T., and Brey G. P., 2005. Subducting
773 oceanic crust: the source of deep diamonds. *Geology*, 33(7), 565-568.
- 774 Taylor H. P., 1977, Water/rock interactions and the origin of H₂O in granitic batholiths. *J. Geol. Soc.*,
775 133(6), 509-558.
- 776 Taylor L.A., and Neal C.R., 1989. Eclogites with oceanic crustal and mantle signatures from the
777 Bellsbank kimberlite, South Africa, Part I: Mineralogy, petrography, and whole-rock chemistry. *J.
778 Geol.*, 97(5), 551-567.
- 779 Taylor L.A., Snyder G.A., Crozaz G., Sobolev V.N., Yefimova E.S., and Sobolev N.V., 1996. Eclogitic
780 inclusions in diamonds: evidence of complex mantle processes over time. *Earth Planet. Sci. Lett.*,
781 142(3), 535-551.

- 782 Taylor L. A., Milledge H. J., Bulanova G. P., Snyder G. A., and Keller R. A., 1998. Metasomatic
783 eclogitic diamond growth: evidence from multiple diamond inclusions. *Int. Geol. Rev.*, 40(8), 663-676.
- 784 Taylor L.A., Keller R.A., Snyder G.A., Wang W., Carlson W.D., Hauri E.H., McCandless T., Kim K-R.,
785 Sobolev N.V., and Bezbobrodov S.M., 2000. Diamonds and their mineral inclusions, and what they tell
786 us: A detailed “pull-apart” of a diamondiferous eclogite. *Int. Geol. Rev.* 42(11), 959-983.
- 787 Tomlinson E.L., Jones A.P., and Harris J.W., 2006. Co-existing fluid and silicate inclusions in mantle
788 diamond. *Earth Planet. Sci. Lett.*, 250(3), 581-595.
- 789 Turner G., Burgess R., and Bannon M., 1990. Volatile-rich mantle fluids inferred from inclusions in
790 diamond and mantle xenoliths. *Nature*, 344(6267), 653-655.
- 791 Viljoen K.S., Schulze D.J., and Quadling A.G., 2005. Contrasting Group I and Group II eclogite xenolith
792 petrogenesis: Petrological, trace-element and isotopic evidence from eclogite, garnet-websterite and
793 alkremite xenoliths in the Kaalvallei Kimberlite, South Africa. *J. Petrol.*, 46(10), 2059-2090.
- 794 Wang S. J., Teng F. Z., Williams H. M., and Li S. G., 2012. Magnesium isotopic variations in cratonic
795 eclogites: origins and implications. *Earth Planet. Sci. Lett.*, 359, 219-226.
- 796 Williams H. M., Nielsen S. G., Renac C., Griffin W. L., O'Reilly S. Y., McCammon C. A., Pearson N.,
797 Viljoen F., Alt J.C., and Halliday, A. N., 2009. Fractionation of oxygen and iron isotopes by partial
798 melting processes: implications for the interpretation of stable isotope signatures in mafic rocks. *Earth
799 Planet. Sci. Lett.*, 283(1), 156-166.
- 800 Zack T., Foley S.F., and Rivers T., 2002. Equilibrium and disequilibrium trace element partitioning in
801 hydrous eclogites (Trescolmen, Central Alps). *J. Petrol.*, 43(10), 1947-1974.
- 802 Zhang H.F., Matthey D.P., Grassineau N., Lowry D., Brownless M, Gurney J. J., and Menzies M.A., 2000.
803 Recent fluid processes in the Kaapvaal Craton, South Africa: coupled oxygen isotope and trace
804 element disequilibrium in polymict peridotites. *Earth Planet. Sci. Lett.*, 176, 57-72.
- 805 Zheng Y.-F., 1993. Calculation of oxygen isotope fractionation in anhydrous silicate minerals. *Geochim.
806 Cosmochim. Acta*, 57(5), 1079-1091.
- 807 Zheng Y. F., Fu B., Gong B., and Li L., 2003. Stable isotope geochemistry of ultrahigh pressure
808 metamorphic rocks from the Dabie–Sulu orogen in China: implications for geodynamics and fluid
809 regime. *Earth Sci. Rev.*, 62(1), 105-161.
- 810

811 FIGURES AND CAPTIONS



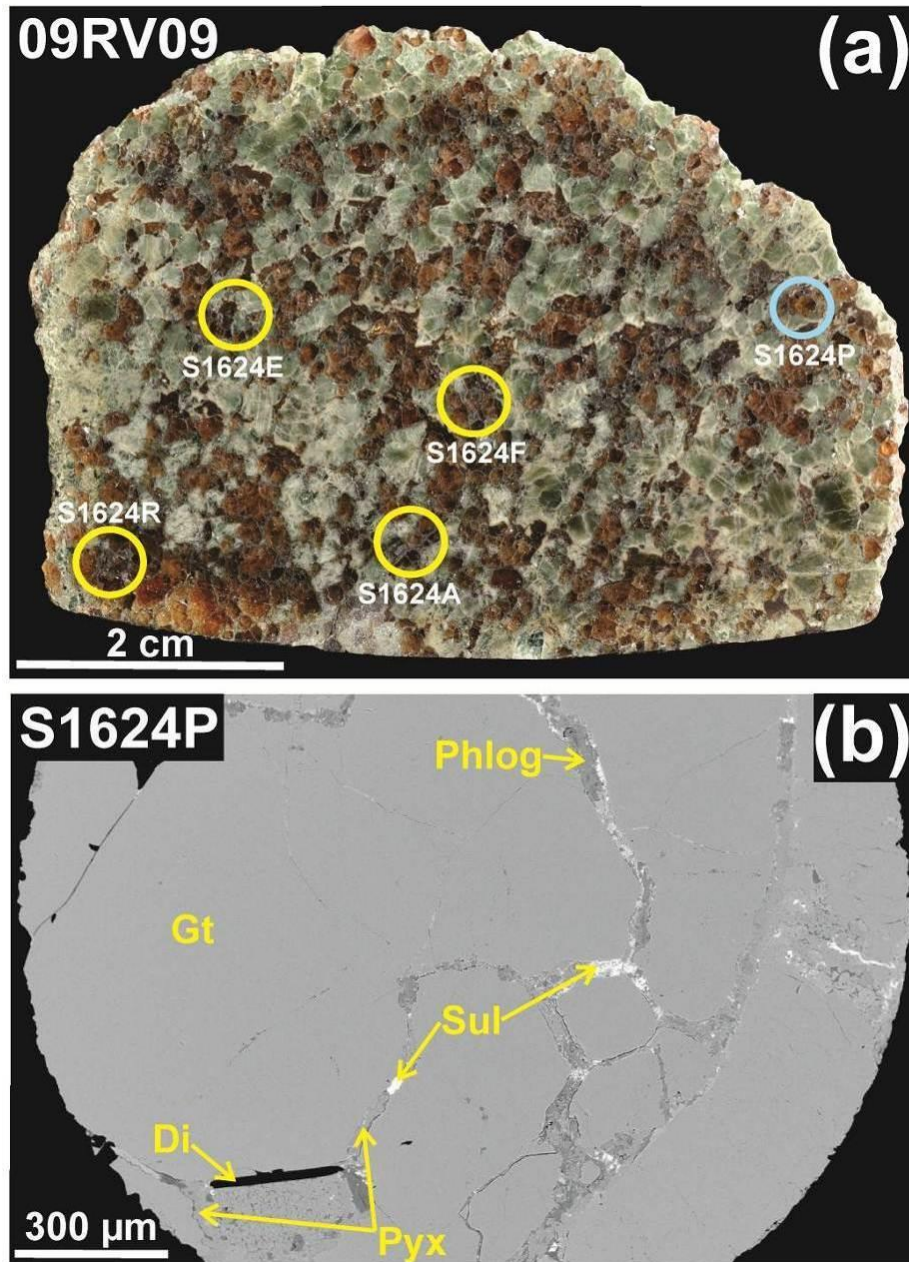
812

813 **Figure 1:** Simplified geological map of south eastern Africa. Location of the Roberts Victor
 814 mine is marked by the red star. This map depicts some of the major structural features within the
 815 Kaapvaal Craton. Image after [Schmitz et al. \(2004\)](#).

816

817

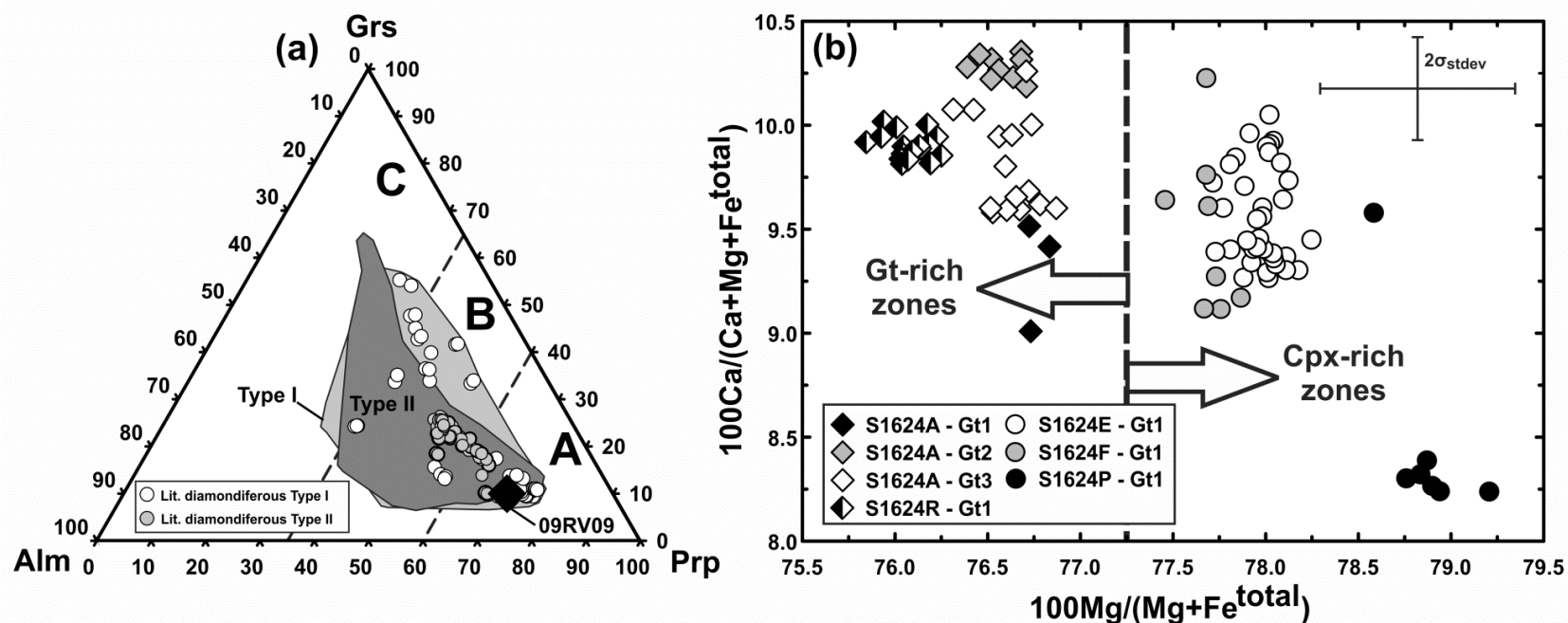
818



819

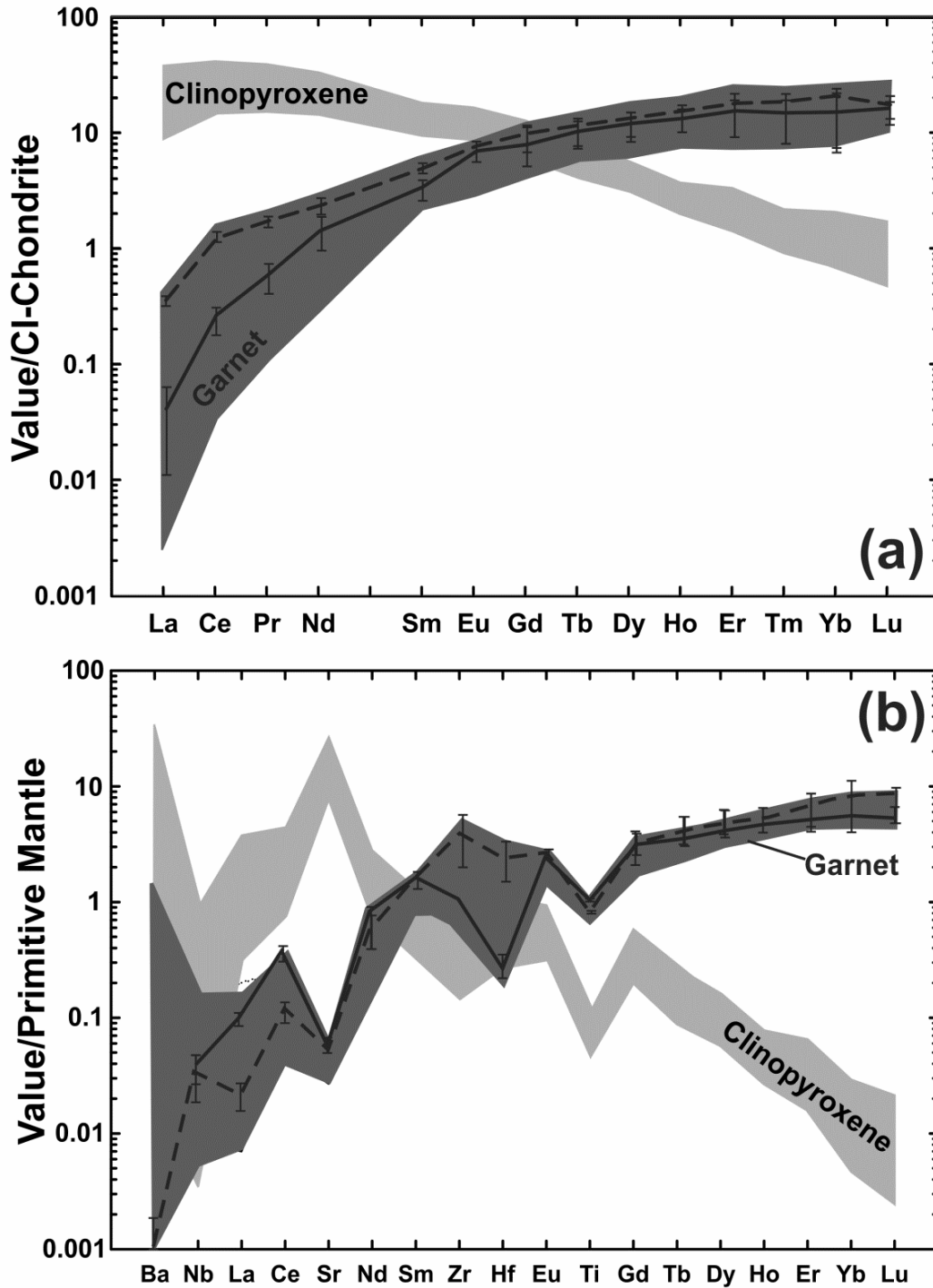
820 **Figure 2:** Hand-specimen (a) and back-scattered electron (BSE) image of 09RV09 (CCIM
 821 sample #S1624). Garnet and clinopyroxene modal abundances are heterogeneously distributed
 822 at the slice and hand-specimen scale. Sample portions extracted for *in situ* analyses are
 823 delineated by yellow and blue open-circles in (a), and S1624X labels correspond to sub-portion
 824 identifiers. The blue circle corresponds to a sample portion in which diamonds was preserved
 825 after polishing. Small diamond successfully retained *in situ* in sub-portion S1624P is intimately
 826 associated with garnet (b). Phase abbreviations are: Gt = garnet, Pyx = pyroxene, Phlog =
 827 phlogopite, Sul = sulphide, Di = diamond.

828



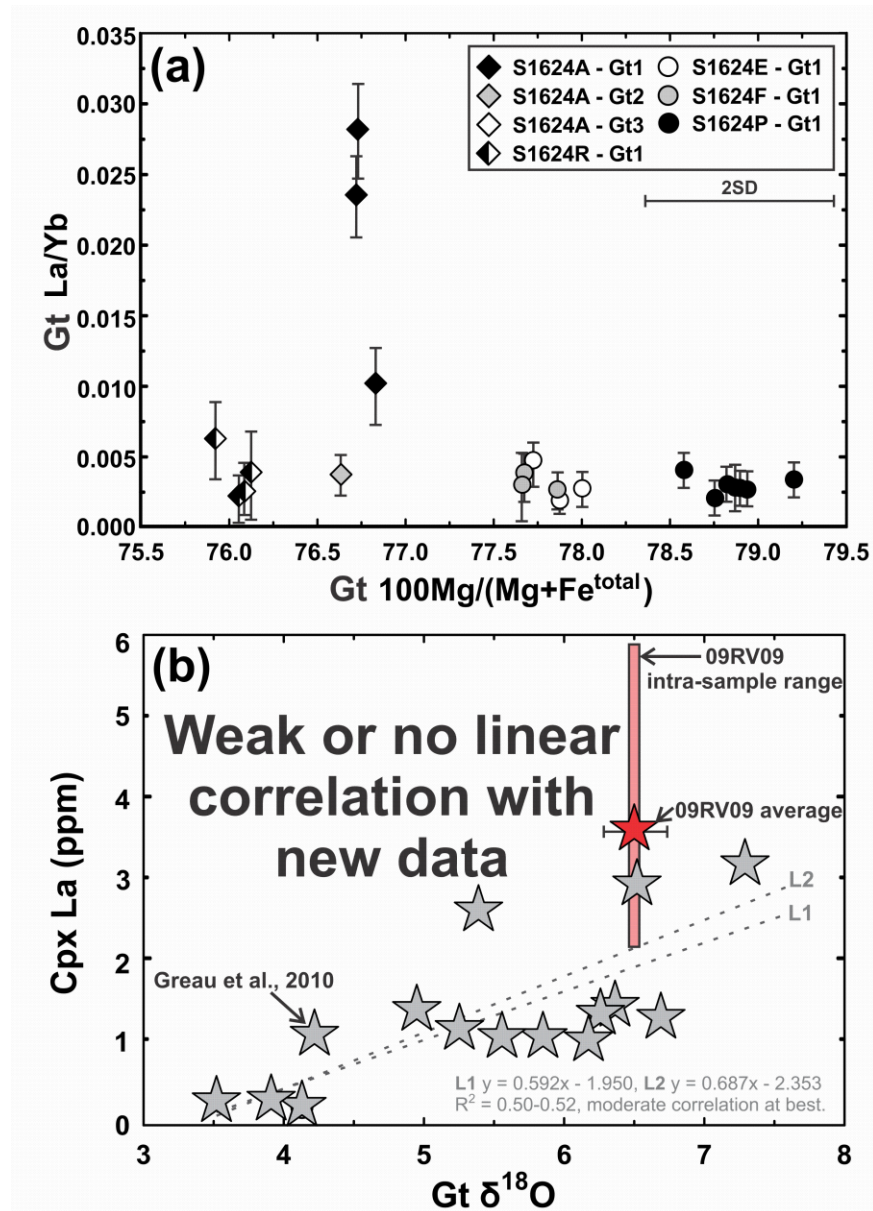
829

830 **Figure 3:** Garnet end-member (a; mol. %) and cation ratios (b). The range of intra- and inter-grain garnet compositions in 09RV09
 831 shown in (a) is enclosed by a black diamond, and these data are compared with the range of garnet compositions reported in previous
 832 studies of Roberts Victor eclogites. Data fields in (a) delineate textural Group I and Group II eclogite xenoliths of Roberts Victor
 833 studied by [Hatton \(1978\)](#). Lit = literature, and corresponds to data reported by [MacGregor and Manton \(1986\)](#), [O'Reilly and Griffin](#)
 834 [\(1995\)](#), and [Gréau et al. \(2011\)](#). The range of intra- and inter-grain major-element cation values in garnets of 09RV09 is shown in (b),
 835 and the standard deviation (SD) was calculated via propagation of typical uncertainties on Ca, Mg, and Fe^{total} (this represents a
 836 minimum value as propagated uncertainties on other cations are not included).



837

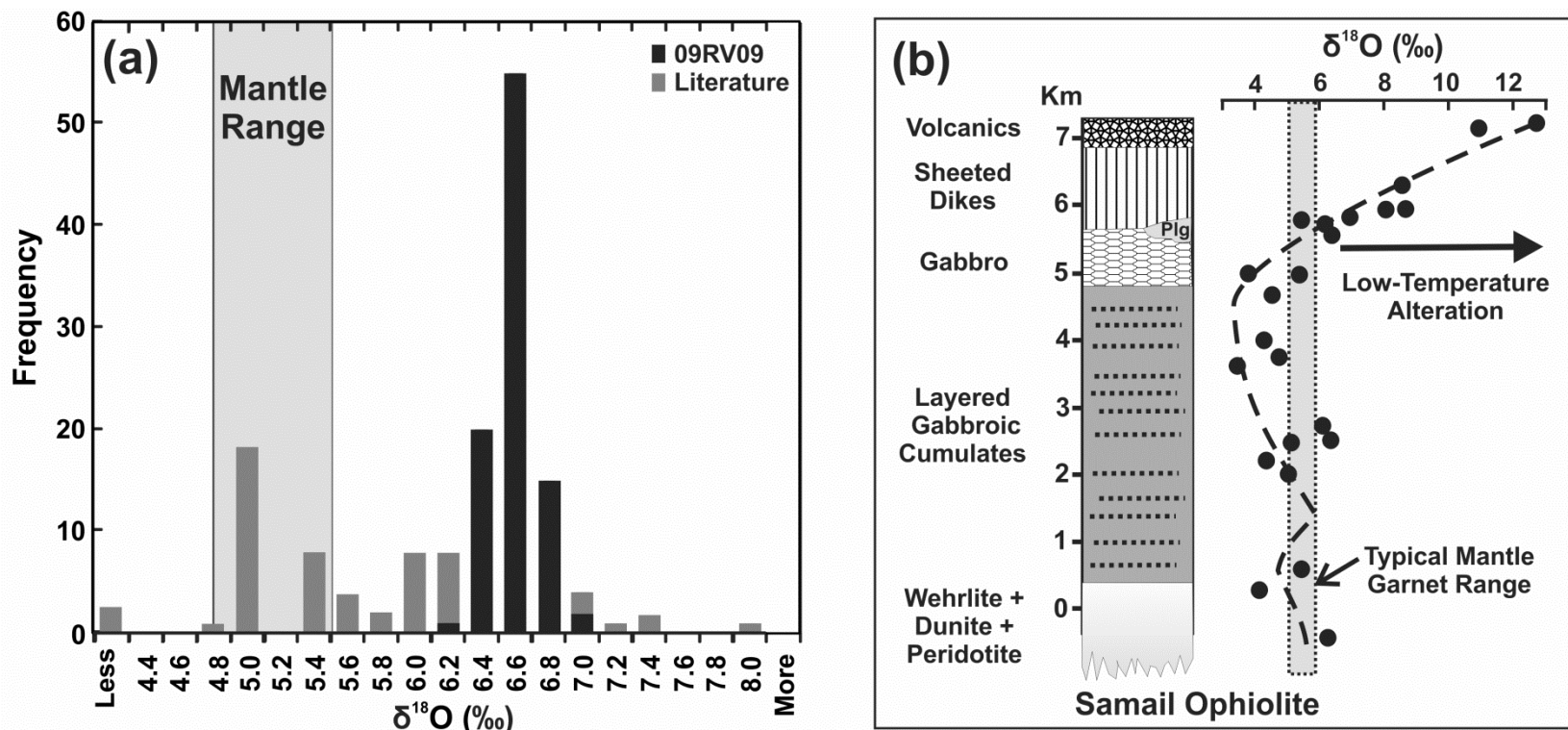
838 **Figure 4:** Rare-earth-element and extended trace-element abundances of 09RV09 minerals
 839 normalised to the values of CI-Chondrite and primitive mantle reported by [McDonough and Sun](#)
 840 (1995). Propagated uncertainties include 2σ precision values determined for each analytical
 841 point. Pm is not measured and is shown as an interpolated space between Nd and Sm (a).



842

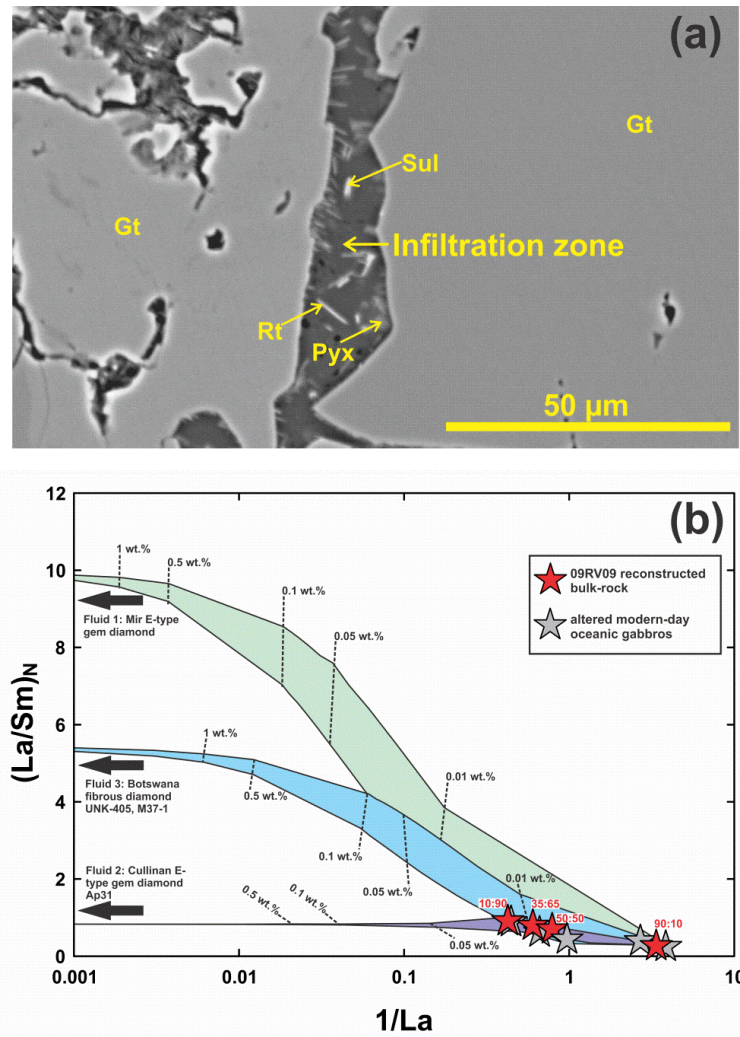
843 **Figure 5:** a) Garnet cation compositions and corresponding La/Yb. Propagated uncertainties on
 844 La/Yb reflect the 2σ internal precision determined for each analytical point. The typical
 845 uncertainty on $100\text{Mg}/(\text{Mg}+\text{Fe}^{\text{total}})$ represents a minimum value as propagated uncertainties on
 846 other cation proportions (e.g., Si) are not included (where SD = standard deviation). b)
 847 Comparison of Roberts Victor garnet oxygen isotope compositions with La abundances of
 848 coexisting clinopyroxenes. Uncertainties on La abundances represent 2σ precision. Linear
 849 regressions of the data of Gréau *et al.* (2010) alone (L1), and incorporating the 09RV09 average
 850 (L2), are not strongly correlated ($R^2 \ll 0.7$). The 09RV09 clinopyroxene La abundance data
 851 range is depicted by the red bar; inclusion of all 09RV09 clinopyroxene La abundance data
 852 (rather than using a single average value) further reduces the correlation coefficient ($R^2 < 0.1$).

853



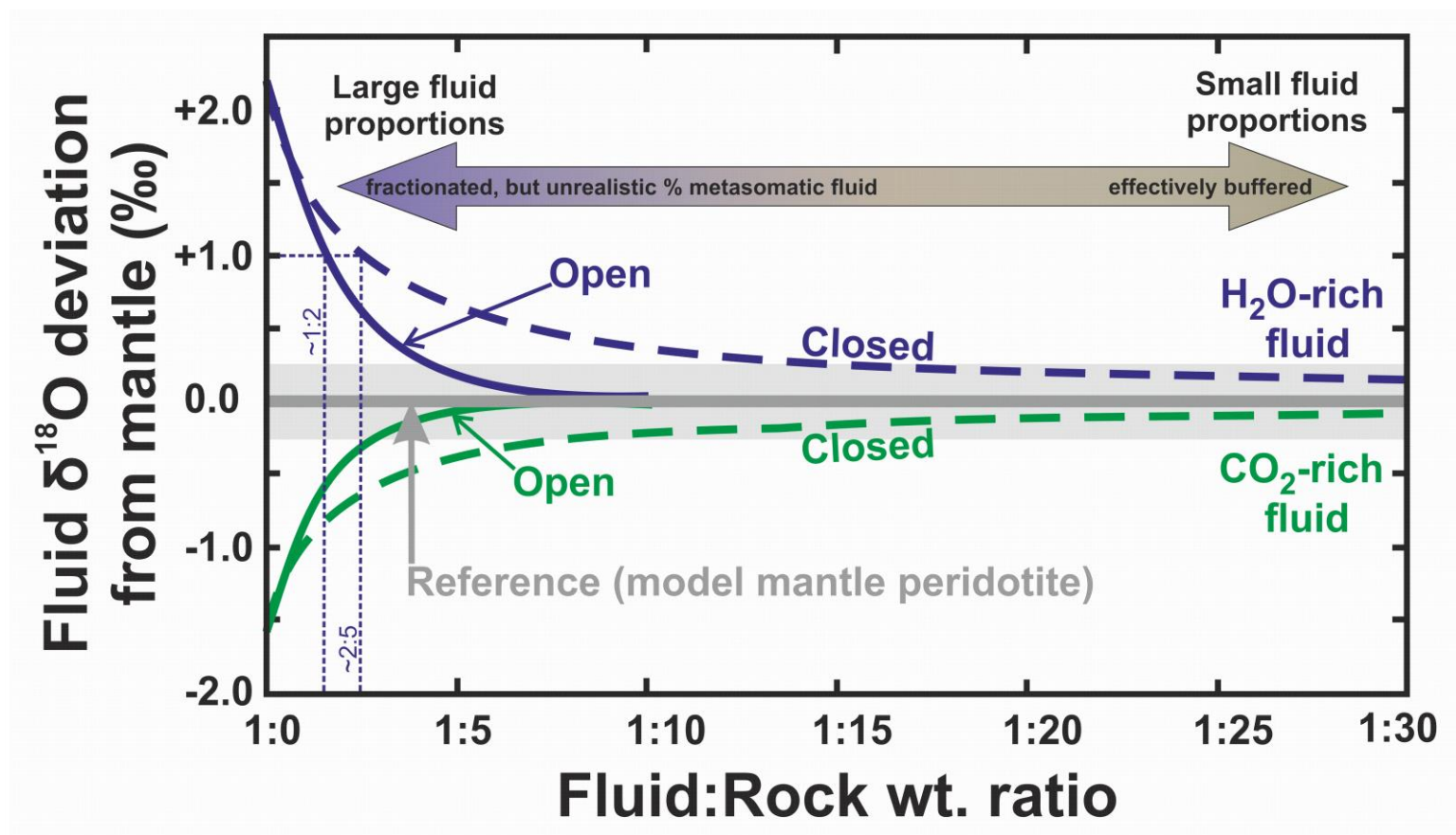
854

855 **Figure 6:** Histogram of oxygen isotope compositions determined for garnets of 09RV09 using ion probe techniques. Literature data
 856 reported for garnet separates of 62 Roberts Victor eclogite xenoliths were sourced from (Garlick *et al.*, 1971; MacGregor and Manton;
 857 1986; Ongley *et al.*, 1987; Caporuscio, 1990; Schulze *et al.*, 2000; Gréau *et al.*, 2011) and the garnet mantle range is after Matthey *et*
 858 *al.*, (1994). A schematic illustration of the range of $\delta^{18}\text{O}$ -compositions determined for samples of the Samail Ophiolite (b); where
 859 $\delta^{18}\text{O}$ -compositions $>+5.9$ ‰ are associated with upper sections of oceanic crust altered at low-temperatures (<350 °C; after Gregory
 860 and Taylor, 1981).



861

862 **Figure 7:** Infiltration and metasomatic modification of 09RV09. a) Narrow infiltration zone and
 863 associated metasomatic phases adjacent to garnet in 09RV09. Gt = garnet, Pyx = pyroxene, Rt =
 864 rutile, Sul = sulphide. The dark grey of the infiltration zone represent quenched material. b)
 865 Reciprocal La abundance (ppm) and CI-chondrite normalised La/Sm values of calculated bulk-
 866 rock reconstructions of 09RV09 over a range of garnet:clinopyroxene ratios compared with
 867 representative compositions reported for relatively fresh and altered gabbros of the slow-
 868 spreading SW Indian Ridge (Hart *et al.*, 1999; Bach *et al.*, 2001). Mixing products determined
 869 for the addition of fluids associated with diamond to these gabbroic compositions, which may
 870 approximate an eclogite protolith, are shown as shaded fields and the percentage of fluid is
 871 marked by dashed lines (refer to [supplementary materials](#) for further details). For visual clarity,
 872 the results of mixing calculations determined for F4 (a fluid with relatively low total REE
 873 abundances) are omitted from this image. Gt = garnet, Pyx = pyroxene, Sul = sulphide, Rt =
 874 rutile.



875

876 **Figure 8:** Model of the effect of closed- and open-system interaction between CO₂-rich and H₂O-rich metasomatic fluids and
 877 peridotite on the fluid $\delta^{18}\text{O}$ -composition. Details of the model are given in the text. The ordinate of the figure is the difference
 878 between the fluid composition and a composition representing a completely rock-dominated system (e.g., where the fluid composition
 879 is fixed by the initial isotopic composition of the peridotite and the fractionation factor). The model curves asymptotically approach
 880 zero, where any initial ^{18}O -enrichment or depletion is effectively erased by equilibration with a large enough volume of rock. The
 881 grey region marks a ± 0.25 ‰ band around the zero value, reflecting a composition that is effectively indistinguishable from one that is
 882 completely rock buffered. Under open-system conditions, and at fluid:rock ratios $< 1:10$, the $\delta^{18}\text{O}$ -value of the fluid is
 883 indistinguishable from the silicate mantle with which it is interacting.

884

885

886

887

888

889

890

891

-end-